A Numerical, Parametric Study of Plasma Contactor Performance

by

John Joseph Blandino

B.S. Aeronautical Engineering, Rensselaer Polytechnic Institute, 1987

SUBMITTED TO THE DEPARTMENT OF
AERONAUTICS AND ASTRONAUTICS
IN PARTIAL FULFILLMENT OF THE
REQUIREMENTS FOR THE DEGREE OF

Master of Science

in

Aeronautics and Astronautics

at the

Massachusetts Institute of Technology

December 1988

Signature of Author _____
Department of Aeronautics and Astronautics
December 1988

Certified by _____
Professor Daniel E. Hastings
Thesis Supervisor
Class of 1956 Career Development
Associate Professor of Aeronautics and Astronautics

Accepted by _____
Wachman
Chairman, Department Graduate Committee

A Numerical, Parametric Study of Plasma Contactor Performance

by

John Joseph Blandino

Submitted to the Department of Aeronautics and Astronautics, January 18,1989, in partial fulfillment of the requirements for the degree of Master of Science

Abstract

In the past decade, a great deal of effort has been dedicated towards the goal of developing alternative power sources for space systems. One such alternative is the electrodynamic tether. The tether system consists of a long conductor which is trailed through the earth's magnetic field by an orbiting spacecraft. The induced Faraday electric field creates a potential difference along the conductor which can, in principle, be used to provide electrical power to a load if a current is established in the conductor.

In order for such a current to flow, an electrical circuit through the ionosphere must be closed. The need to establish electrical "contact" with the ionosphere has led to the study of "plasma contactors" which are plasma sources capable of emitting ions to, or collecting electrons from, the ambient plasma. One type of plasma source which has been considered for use as a contactor is the hollow cathode. Efficient contactor design is key to electrodynamic tether system operation.

Some experimental and theoretical treatments of plasma contactors are outlined and reviewed. In particular, the definition of a one-dimensional core plasma cloud in the vicinity of the contactor is discussed and a numerical model formulated. Two criteria

for determining an upper and lower bound on the core cloud radius are discussed. This model is then used to investigate the influence of various system parameters on contactor performance.

Two figures of merit are considered in assessing contactor performance. These are the potential drop across the core cloud, and the degree of current enhancement or gain associated with operation at any given set of conditions. In addition the radius of this core cloud is determined. The parameter space investigated includes variation of contactor ion current ($10mA - 1A$), ambient ion density ($10^9 - 10^{13}m^{-3}$), electron temperature at the contactor ($0.5 - 10eV$), and initial ion injection mach number ($0.5 - 10$). In addition the effect of varying contactor radius, degree of ionization, and presence of anomalous resistivity is explored.

It is found that potential drops were most sensitive to variations in electron temperature in the vicinity of the contactor varying by roughly $60V$, whereas variations in ion current, ambient density, and initial mach number produced the much smaller variations of $2V$,$3V$, and $1.0V$, respectively.

Current enhancement or gain is found to be most sensitive to variations in ion current varying by a factor of about 3.5 over the range of currents spanned. Spanning four orders of magnitude in ambient density results in changes in the gain which are less than a factor of 3. The gain is found to be much less sensitive to changes in the other parameters varying less than a factor of 2 with electron temperature and mach number.

The cloud radius is found to vary from roughly $3m$ at the high end of ambient densities considered to roughly $40m$ for the lowest densities. The variation with ion current, electron temperature and ion mach number is much smaller. Increasing ion current results in an increase in radius by a factor of less than 4 while variations in electron temperature and mach number result in changes of less than a factor of 2.

These results as well their implications for contactor design and testing are outlined and discussed.

Thesis Supervisor: Daniel E. Hastings, Class of 1956 Career Development Associate Professor of Aeronautics and Astronautics

Acknowledgements

I would like to offer my sincerest thanks to Professor Daniel Hastings for his many suggestions, help and guidance. In particular I am greatful for his unwavering support and patience during my introduction to the field of plasma physics.

I would also like to thank my fellow graduate students who were extremely helpful throughout the past year by sharing their experiences, advice, and expertise in a variety of areas. In particular I would like to thank Mark Lewis, Nick Gatsonis, Jiong Wang and Patrick Chang. The past year has been significantly enriched by their friendship and support.

Finally I would like to offer my most heartfelt gratitude to Pamela Cooley for her unfailing confidence, support and help in completing this thesis.

Contents

List of Figures

Chapter 1
Background

1.1 Electrodynamic Tethers and the Motivation for Contactors

Electrodynamic tethers are a power conversion system by which either electrical energy is changed into orbital kinetic energy or orbital potential energy is converted into electrical energy. In this system, a long conductor is trailed from a spacecraft while in orbit (Figure 1.1)where it can interact electromagnetically with the ionosphere. One attractive feature of a tether system is its ability, in principle,thereby to operate in either an electrical power production mode or in a thruster mode. In the power production mode, the Faraday electric field given by $\vec{v} \times \vec{B}$ where $\vec{v}$ is the orbital velocity and $\vec{B}$ is the geomagnetic field vector, will establish a potential difference along the length $\vec{l}$ of the conducting tether. The magnitude of this potential is in turn given by the expression $V_{oc} = (\vec{v} \times \vec{B}) \cdot \vec{l}$. This represents the open circuit voltage which would exist across the the two ends of the tether. If the circuit is closed and a current I allowed to flow, orbital energy can be converted into electrical energy at the rate $P = IV_{oc}$ where P represents the power being converted. Such a current loop can be established if the tether can make electrical "contact" with the ionosphere and in this way form a complete circuit. Various classes of devices have been proposed to effect

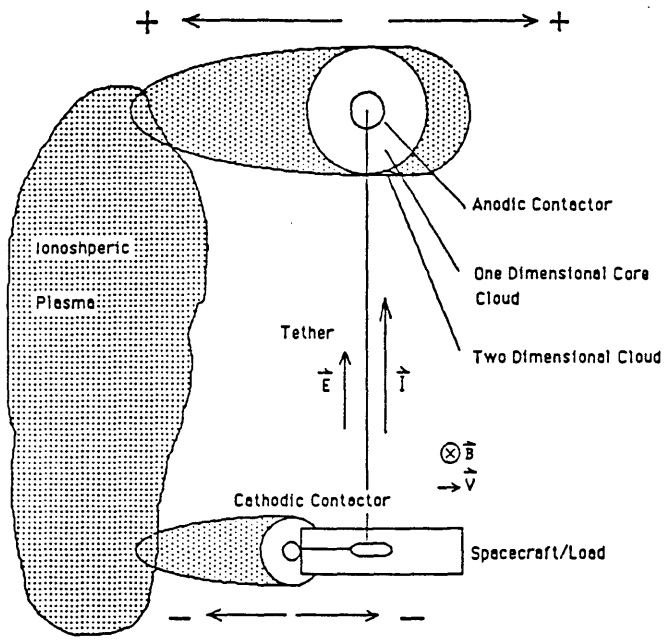

Figure 1.1: Schematic of Spacecraft-Tether-Ionosphere System

this electrical contact. One class of devices which utilize an artificially generated plasma cloud have been referred to as "contactors" in the literature and will be referred to as such in this thesis.

In the thruster mode of operation an on-board power supply provides a large enough potential to overcome the induced open circuit potential and set a current flowing in the opposite sense through the loop. This has the effect of creating a force, the magnitude of which is given by the Lorentz force equation as $\vec{F} = \vec{I} \times \vec{B}$ which serves to exchange momentum with the ionospheric plasma and thereby change the kinetic energy of the spacecraft. It should be evident that such a reversible power system could have potential application to a number of power generation and storage needs as well as orbit maintenance/modification. These mission applications have been studied in some detail in the literature [10]. Among possible tether system applications are the following:

- Drag Compensation
- Orbit Altitude/Inclination Changes
- Power Generation (emergency or stand alone)
- Energy Storage for Solar, Battery, or Fuel Cell System

It was mentioned previously that for a tether system operating in power generation mode, orbital energy can be converted into electrical energy at a rate equal to the product of the open circuit voltage and the current in the circuit $P = IV_{oc}$. It is likely, however, that the useful voltage drop across the load will be substantially less than the open circuit voltage. The reason for this is that there will be some non-zero impedance and corresponding voltage drop associated with the various elements of the tether system. In particular, there will be a voltage drop ΔV_t associated with the tether wire, the anodic and cathodic contactors at each end $\Delta V_a, \Delta V_c$, and some loss due to the impedance of the ionosphere itself ΔV_i. An efficiency can now be defined as the ratio of electrical power available to the load to the power extracted from orbit

$$\eta = V_L / V_{oc}$$

which can be written

$$\eta = \frac{V_L}{V_L + \Delta V_t + \Delta V_a + \Delta V_c + \Delta V_i}$$

The voltage drop associated with the ionospheric plasma ΔV_i will in general be small compared with other system elements and cannot in any event be directly controlled. While the ΔV_t associated with the tether conductor can in fact be controlled through choice of material and wire size, there are a number

of other factors which must be considered as well. These include mechanical stability, insulation requirements, redundancy to protect against single point failures (such as meteor impact) and system mass constraints. These competing system issues effectively predicate the lower bound on the tether impedance and hence ΔV_t as well. As a consequence, the system efficiency η will in large part be determined by the contactor voltage drops ΔV_a and ΔV_c. Minimizing these voltage drops then becomes a critical design requirement since the entire system efficiency is driven by the contactor impedance. For a feasible system then, most of the parasitic voltage drop should occur across the electrodes which can in some measure be controlled, so that we can write,

$$V_L \gg \Delta V_a + \Delta V_c \gg \Delta V_t + \Delta V_i$$

or

$$\eta \approx \frac{1}{1 + (\Delta V_a + \Delta V_c)/V_L}$$

The sensitivity of this conversion efficiency to contactor performance underlies the necessity to minimize the voltage associated with their operation. A system goal is then to decrease the contactor operating voltage without incurring too large a penalty in terms of system mass or reliability.

The relation of the various voltage drops associated with a tether system are depicted graphically in Figure 1.2 from ref [10]. In this figure $\vec{B}$ is oriented into the plane of the page while the orbital velocity vector $\vec{v}$ points to the right. The electric field $\vec{E}$ in the reference frame of the tether as well as well as the induced current $\vec{I}$ will then point upwards in the case of the generator Figure 1.2 a), and downwards in the case of the thruster Figure 1.2 b). It is useful to consider some typical numbers for the quantities involved in order to get a sense of the contactor performance characteristics which comprise the topic of this thesis.

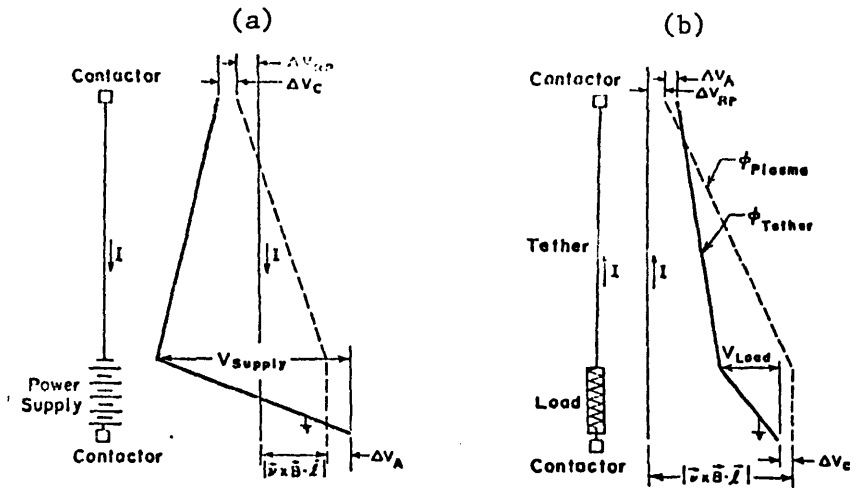

Figure 1.2: Potential Diagram for Tether as a)Generator and b) Thruster

For a fully operational space station, the required electrical power is generally accepted to be at least on the order of $100kW$. In low earth orbit the magnitude of the earth's geomagnetic field is approximately $0.5 \times 10^{-4}T$. With an orbital velocity of $8km/s$ and a tether length of of $10km$, one could expect open circuit voltages of about $4000V$. For a $100A$ current, a $100kW$ system could operate at an efficiency as low as 0.25 or $\Delta V_a + \Delta V_c \approx 3000V$. In general, the losses in the tether ΔV_t will increase as the square of the current in which case our assumption $\Delta V_a + \Delta V_c \gg \Delta V_t$ may not be valid for a current as high as $100A$. To minimize these dissipative losses then, currents on the order of tens of amperes are considered more reasonable. Lower currents require higher efficiency for a given power to the load. To operate at the same power level at a current of only $30A$ for example, would require an efficiency of 0.83 to obtain the required voltage drop across the load. The corresponding voltage drop permissible across the contactors is then approximately $683V$. Hence the need to operate at low currents and high power levels underlies the need for high system efficiencies and low contactor operating voltages. In addition, high efficiencies are required if the tether power system is to be a viable alternative to existing power systems such as fuel cells and solar arrays.

The device ultimately chosen for use as a contactor will depend upon a variety of system level considerations such as mass, reliability, consumables required, etc. Various options could conceivably fulfill this role although a few stand out as holding more promise [10]. In steady state operation, these devices should not require a separate neutralizing current since presumably ions emitted at the anode are compensated by an equivalent current of electrons emitted at the cathode. Two possibilities for cathodic contactors include an electron gun and hollow cathode plasma source. The electron gun has the advantage that it does

not require consumables and is technologically mature. However, it operates at high voltage and would therefore be too inefficient for a tether application. Hollow cathodes create a plasma from which electrons (when operating as a cathode) or ions (when operating as an anode) can be emitted selectively. In principle it has the further advantage of relatively low voltage drop as well as the capability of operating as either an anode or cathode. The primary disadvantages associated with the hollow cathodes are a non-zero mass flow rate required to create and sustain the plasma, as well as their relative technological immaturity.

For the anodic contactor, (ion emitter or electron collector), the options are somewhat more varied. For a passive system such as a large surface or grid, the collected current is limited by the random current $j_r = en_e(\bar{c}_e/4)A$, where n_e is the ionospheric electron density, A is the collecting surface area, and $\bar{c}_e$ is the mean velocity for a Maxwellian distribution. For average values of $n_e \approx 10^{11}m^{-3}$, and $T_e \approx 0.1eV$, the current density is $j_r = 0.8mA/m^2$. For a system power of $100kW$ and open circuit voltage of $5000V$ a current of $20A$ is required assuming perfect efficiencies. If our collecting surface was a sphere such as a metallic balloon, this would require a diameter of $178m$ ($A_{coll} = 25,000m^2$). The dynamic requirements of such a large object such as neutral drag compensation make such an alternative unfeasible. While a wire mesh system could provide somewhat of an improvement in terms of drag, it has the disadvantage, as does the large metallic balloon, that it cannot be used reversibly in a thruster mode.

To overcome the low value of the ionospheric random current , one must enhance the effective collection area by providing some means of current amplification or gain. One way this can be accomplished is through the use of hollow

cathode plasma sources which have already been discussed. Hollow cathode plasma sources overcome the limitation set by the low value of random thermal current density in two ways. First, they emit a plasma cloud which serves to increase the "effective" area over which current collection can take place. This is a consequence of the randomizing collisions which create a roughly spherical diamagnetic cloud which can be many times the size of the contactor itself. Since electrons drifting into this cloud are not constrained to move along the magnetic field lines, the collisional "core" cloud enables the collection of electrons from the far field travelling in a flux tube intersecting the cloud (Figure 2.1). The second effect, which only becomes important for larger currents and higher electron temperatures is ionization of neutrals in the core cloud. Ionization of neutrals produces an additional means of amplifying the current collected by one of these devices. While still in need of further development, hollow cathode plasma sources hold a great deal of promise. They are particularly attractive for a tether system designed to operate in both power production and thruster mode since the direction of current flow can be reversed.

1.2 Contactor Research

The concept of using hollow cathode plasma sources as contactors grew out of the need to achieve low impedance electrical contact with the ionosphere as well as reversibility of operation (i.e., as either anode or cathode). Much of the theoretical treatment of these devices comes from an extension of space charge limited flow theory for which there is a substantial body of literature. Katz [9] provides an introductory treatment of the hollow cathode plasma emitter as a contacting device. While this treatment did not account for the presence

of a magnetic field nor the formation of double-layers, it did demonstrate the potential for low impedance current collection in theory.

Dobrowolny and Iess [2] have obtained an approximate analytical solution for the potential profile of a hollow cathode plasma. In their work they have considered the case of monoenergetic ions expanding under the influence of a positively biased anode. Density of ambient ions, assumed Maxwellian, is taken to decrease exponentially and the electron density obtained by assuming quasineutrality throughout the expanding cloud. With these assumptions they are able to obtain a first order nonlinear equation for the plasma potential. To obtain an analytical solution to this problem the expanding cloud is divided into three regions. In the inner-most region where the electrons are suprathermal, momentum transfer is assumed dominated by collisions brought about by an ion-acoustic instability. In addition, pressure gradient and inertial terms are neglected. The intermediate region is characterized by the inclusion of a pressure gradient and frictional terms although still considered to be non-inertial. In the outermost region, only the frictional terms are neglected. One goal of this work was the estimation of gain or enhancement factors (ξ) defined as

$$\xi = \frac{I_{collected}}{I_{emitted}}$$

While preliminary, the analysis did obtain estimates of the quasineutral potential profile as well as current enhancement factors. A typical value would be $\xi \approx 50$ for a contactor operating at a potential bias of $100V$ in an ambient plasma of $10^9 cm^{-3}$. The corresponding emitted ion current is roughly $70mA$. The analysis however did not include the inherent multidimensional effects which arise as a consequence of the magnetic field. In their conclusions, the authors acknowledge that actual enhancements would be much lower since the expan-

sion would only be one-dimensional in the inner-most region. In their treatment the current enhancement was treated as an eigenvalue of the model formulation and solved for explicitly. This differs from other formulations [6] in which the enhancement is determined from the random electron flux incident upon a core defined on the basis of physical considerations. While determining this enhancement from the mathematics has the advantage that it is obtained directly, one must be very careful when interpreting these results since the area over which effective current collection can occur is consequently not well defined. In the absence of ionization it is collection of electrons from the far field which will ultimately provide the current amplification. In this respect the gain and core radius must ultimately be related. Wei and Wilbur [16] investigate the problem of double layer formation in a spherical geometry with counter streaming particle currents. This is in contrast to the previously cited reference where the plasma is assumed to expand into a quiescent background of Maxwellian ions. Extension of this theoretical treatment into a genuine multidimensional framework which includes the asymmetry imposed by the geomagnetic field has been done by Hastings [5][6]. In this work, which addresses some of the limitations of contactors specific to space operation, the plasma cloud is divided into three regions.

The inner most region is a dense, highly collisional core where the directionality imposed by the earth's magnetic field is destroyed and expansion is radial only. There are several methods for defining the boundary of this core which will be discussed in more detail later. In general, however, this inner region is defined by the condition that both electrons and ions expand under the dominant influence of the applied electric field. In addition, the region is sufficiently collisional that neither species is constrained to move along the magnetic field lines.

In the middle or transition region, the ions have become magnetized though the electrons are still moving predominantly under the influence of the electric field. The boundary of this transition region with the outermost is defined by the condition that electrons are magentized as well. In this outer region the effects of both the magnetic and electric fields are manifested in the plasma. It is only in this region that the asymmetry imposed by the drift of the tether system through the ionosphere is evident.

Unfortunately there has not been a great deal of experimental work performed to study the behavior of plasma contactors in terrestrial laboratories and even less in space. Wilbur and Williams [17] have performed some ground based laboratory tests of contactor performance utilizing hollow cathodes. In these tests one hollow cathode plasma source was used as a current collecting device and another to produce a simulated ambient plasma environment in the vacuum tank. These experiments were characterized by the formation of a double sheath in the vicinity of the contactor as well as the triggering of an "excited" mode of operation in which atomic excitation collisions result in a luminous region. A simple theoretical model based on space charge limited flow was found to predict the location of the sheath radius within a twenty-five percent margin of error. In this model, the potential gradients observed corresponded to three distinct regions which have been repeatedly observed in ground based laboratory experiments. In the innermost region consisting of a high density plasma plume, there is a small potential gradient which extends radially outward to a distance on the order of 10cm for a discharge current of approximately 0.3A. This is followed by a double sheath region with a potential drop on the order of tens of volts. With sheath thicknesses on the order of a few centimeters, the corresponding electric fields were estimated to be on the order of several thou-

sand volts per meter. In the outermost or ambient plasma region the plasma is assumed uniform and Maxwellian. The potential gradient is very weak in this region as well.

In further work by the same investigators [18] the $I - V$ characteristics for these devices were mapped out with typical values on the order of several tens-of-volts for ampere level currents. In addition it was observed that the contactors operated more efficiently in the "ignited" mode. While this work provided some sorely needed data for validation of theoretical models and computer codes, it did raise some important questions concerning the applicability of ground based test data to actual projected operation in the ionosphere. In particular, Katz and Davis [8] demonstrate that the sheath radius in these previously discussed experiments could very easily have become larger than the vacuum tank itself. The fact the ambient density in the tank may have been artificially higher than would actually have been encountered in space would have resulted in a smaller sheath and hence affected some projections of the sheath structure. In addition, it has been suggested [5] that the use of hollow cathode ion emitters to generate the ambient plasma in these experiments may have contributed to the formation of the observed double layers since the incoming electrons are already accelerated to supersonic speeds. In the absence of double layers in the far field, electrons would normally be subsonic in the space environment.

Vannaroni and his colleagues at The Institute for Interplanetary Space Physics at Frascati have conducted some plasma diagnostic experiments using hollow cathode sources [3]. These preliminary experiments investigated the plasma characteristics associated with a hollow cathode operating in an evacuated chamber in the absence of a magnetic field or ambient plasma. Using two spherical

Langmuir probes, this work identified two Maxwellian electron populations with temperatures of approximately 0.5 and 10eV. Additional experiments by this group have been conducted in the large Frieburg plasma chamber which included a simulated ambient plasma environment. These results indicated an enhancement of total current for a hollow cathode operating as a plasma source over one in which the device is only biased with respect to the backround plasma. Additional work by the European Space Agency has extended these simulations to include magnetic field effects perpendicular to the direction of plasma flow [15]. In this work, Lebreton and colleagues observed a reduction in electron current collection when this collection occurred in the presence of a transverse magnetic field. These experiments also investigated the behavior of a sheath region in a magnetic field.

1.3 Scope of Present Work

The work described in this thesis sought to expand the understanding of plasma contactor performance by investigating an extended parameter space. The results presented here were based on a one-dimensional computational model which solved the radial plasma dynamic equations for a plasma under the influence of an applied electric field. Contactor performance was characterized by two figures of merit, the current enhancement or gain, and the minimum potential drop required for the associated gain. In addition the dimensions of the core cloud were investigated and results using two different models for the core evaluated.

The sensitivity of contactor performance to variations in four parameters was

sought in detail. These were: the contactor ion current, ambient ion density, electron temperature at the contactor, and ion injection mach number. The influence of three additional variables was investigated to somewhat of a lesser extent. These were the initial degree of ionization for the emitted plasma, the presence of anomalous resistivity, and the assumed radius of the hollow cathode emitter. The significance of this last feature lies primarily in its importance for correlation of experimental work and numerical simulation. In general hollow cathodes are not spherical emitters; nevertheless, it is assumed for simplicity in the problem formulation that the plasma cloud geometry becomes spherical beyond a certain radius. It is the sensitivity of the results to this assumed radius that was briefly investigated here.

Finally, it is important to delineate the scope and limitations of the model presented. The model consisted of a three species plasma composed of argon ions emitted from the contactor, singly ionized ambient oxygen ions, and electrons. While the atomic oxygen ions would in general be Maxwellian and influenced by the presence of the positively biased contactor, they were assumed to be unperturbed and provide a uniform background. The reason for this was that the contactor plasma was, in general, denser than the background by a factor of several thousand; in addition, the density for these ions can be described by an expression of the form

$$n_{O^+}(r) = n_{O^+}(\infty) exp(-e\phi/T_i)$$

For most of the cases considered, $e\phi/T_i \gg 1$ so that the density of oxygen ions in the core cloud as given by the above expression was negligible.

As mentioned, a figure of merit was the minimum potential drop associated with the contactor for a given gain. The fact the potentials calculated were

the minimum possible is a direct consequence of the fact quasineutrality was imposed throughout the solution of the core region. This assumption precludes a double layer structure and therefore will not reflect the substantial potential drops which can occur and which have been observed to occur with these devices.

In view of this fact one may well ask to what extent can the present analysis be expected to reflect the actual plasma contacting process. From a systems standpoint, the minimum potential drop associated with a given set of operating conditions is significant since it represents an upper limit on the obtainable performance (minimum impedance). In addition, there is presently a lack of experimental work which can be truly considered representative of the ionospheric environment. This is significant since the sheath structure observed in terrestrial laboratories has yet to be completely understood. In particular there is some question as to the role the source used to simulate the ambient plasma may be playing in forming and sustaining these double layers. If such sources (Kauffmann, for example) are providing a supersonic electron population these may be playing a significant role in sheath formation. In the absence of any accelerating mechanism in the far field, such a population would not be present in the space environment.

Chapter 2
Theory and Model Development

2.1 Definition of the Core Region

Previous work has explored the various plasma cloud regions associated with the contacting process [6]. As mentioned previously the inner-most region consists of a diamagnetic, dense, highly collisional core where both electrons and ions are unmagnetized. The present study focused exclusively on the behavior and characteristics of this core cloud. The intermediate or transition region represents the point at which the electrons become magnetized although expansion is still dominated by the applied radial electric field. The question then arises as how best to define this point of transition. The present work considers two approaches which are shown to yield an upper and lower limit on the size of this one-dimensional core cloud.

The first criterion is a macroscopic condition which states that the radial drift of the electrons in the contactor potential field exceeds the motional $\vec{v_e} \times \vec{B}$ drift due to the magnetic field. The statement of this condition is the requirement that $E/vB = 1$, where E is the radial applied electric field, and v is the electron drift velocity. In this collisional core the plasma pressure is greater than the magnetic pressure implying the cloud is diamagnetic. For this reason the magnetic field used in the above relation is the diamagnetically modified field.

An additional consequence of a magnetic field is the entrainment of electrons into their gyro-orbits. This microscopic condition, therefore, provides an alternative means of delineating the boundary of the one-dimensional core cloud. In this case the boundary is determined by the requirement that the cloud is sufficiently collisional to insure radial expansion. The statement of this condition is the requirement that $\nu/\omega = 1$ where ν is the total electron momentum transfer collision frequency and ω is electron gyrofrequency based on the diamagnetically modified field. This condition is referred to as the collisionality condition and provides a lower bound on the core radius.

Some authors have suggested a core boundary based upon the condition that the contactor plasma density reach the ambient density [9]. While it is true the contactor ion density must ultimately reach the ambient, there is no guarantee this will occur within the one-dimensional region. Some simulations of expanding plasma clouds beyond the core region indicate formation of cigar shaped structures as expansion becomes two dimensional [6].

It is possible to relate the two core criteria by examining a simplified form of the electron momentum equation [6]. If we neglect the inertial terms and assume constant temperature we can write

$$0 = -T_e \frac{\partial n_e}{\partial r} - e n_e E + m_e n_e \nu_{ei}(v_i + v_e) + m_e n_e \nu_{en}(v_n + v_e)$$

where the above scalar equation assumes the electrons are counter-streaming to the other plasma species. If we write $\nu_e = \nu_{ei} + \nu_{en}$ then we can rewrite the equation

$$0 = -T_e \frac{\partial n_e}{\partial r} - e n_e E + m_e n_e \nu_e v_e + m_e n_e (\nu_{ei} v_i + \nu_{en} v_n)$$

Dividing through by $n_e v_e B$ and recalling the cyclotron frequency is defined as

$\omega = eB/m_e$ we can rewrite the equation again as

$$\frac{E}{v_e B} = \frac{\nu_e}{\omega} - \frac{T_e}{ev_e B}\frac{\partial}{\partial r}(\ln n_e) + \frac{1}{\omega v_e}(\nu_{ei}v_i + \nu_{en}v_n) \tag{2.1}$$

Since the electron density gradient will always be negative in this core cloud each term on the right side of the above equation will be positive. It is thus evident that while $\nu_e/\omega \geq 1$ implies $E/v_e B \geq 1$ the converse is not true. From this it is concluded that the collisionality condition will provide a more conservative estimate of the core radius than the electric field condition [5]. The remaining equations to be satisfied within the core cloud will now be developed.

2.2 Governing Equations

2.2.1 Contactor Neutrals

An expression for the contactor neutral density can be obtained from the continuity equation:

$$\frac{1}{r^2}\frac{\partial}{\partial r}(r^2 n_n V_n) = S_r - S_i$$

where the ionization and recombination rates are defined as

$$S_i = n_n n_e \langle \sigma v \rangle_i$$

$$S_r = n_i n_e \langle \sigma v \rangle_r$$

The ionization and recombination rate terms $\langle \sigma v \rangle_i$ and $\langle \sigma v \rangle_r$ (no. of collisions $\cdot m^3/sec$) are given by

$$\langle \sigma v \rangle_i = \frac{10^{-11}}{\sqrt{\gamma}} \frac{exp(-\gamma)}{E_{ion}^{\frac{3}{2}}(6 + 1/\gamma)}$$

from Ref. [11] and

$$\langle \sigma v \rangle_r = 5.2 \times 10^{-20} \sqrt{\gamma}(0.43 + 0.5\log(\gamma) + 0.469/\gamma)^{\frac{1}{3}}$$

from Ref. [14]. In these expressions, γ is the dimensionless ratio of ionization energy to electron energy E_{ion}/T_e, each measured in electron volts.

Expanding the continuity equation,

$$\frac{1}{r^2}[r^2(n_n \frac{\partial V_n}{\partial r} + V_n \frac{\partial n_n}{\partial r}) + 2r n_n V_n] = S_r - S_i$$

The neutral atoms are assumed Maxwellian and taken to expand solely as a result of a density gradient in the vicinity of the contactor. Since the neutral

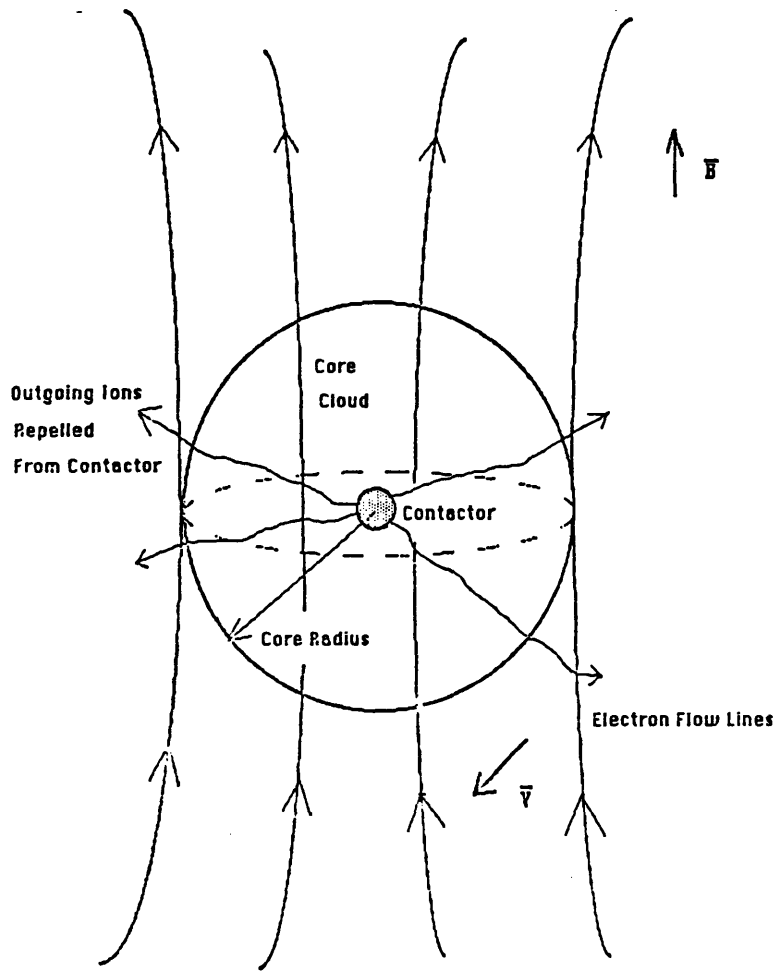

Figure 2.1: Core cloud surrounding plasma contactor showing electron and ion flow lines

velocity is only affected by collisions with the ions and electrons, their mean velocity is taken to be relatively constant and the velocity gradient term is neglected.

$$\frac{\partial n_n}{\partial r} = \frac{S_r - S_i}{V_n} - \frac{2n_n}{r} \tag{2.2}$$

2.2.2 Electric Potential

Writing the electron momentum equation in vector form will allow us to obtain an expression for the potential gradient. In this formulation, the ions are taken to drift outward in the $+\vec{e}_r$ direction while the electrons are drifting inward from the far field in the $-\vec{e}_r$ direction. In demonstrating the relative magnitudes of the E/vB and ν/ω stoppping conditions previously, a limited form of the electron momentum equation was considered. We now write the complete form of the equation including inertial and temperature gradient terms.

$$m_e n_e \vec{V}_e(\vec{\nabla} \cdot \vec{V}_e) = -\vec{\nabla} P + e n_e \vec{\nabla} \phi + \sum_i m_e n_e \nu_i (\vec{V}_i - \vec{V}_e)$$

The first term is the momentum convection term. With $\vec{V}_e = -V_e(+\vec{e}_r)$ it can be expanded to give:

$$\vec{V}_e(\vec{\nabla} \cdot \vec{V}_e) = V_e(\frac{\partial V_e}{\partial r} + \frac{2V_e}{r})\ (+\vec{e}_r)$$

The pressure force term is due to temperature and density gradients. This term becomes, with temperature in units of energy,

$$-\vec{\nabla} P = (-e n_e \frac{\partial T_e}{\partial r} - e T_e \frac{\partial n_e}{\partial r})\ (+\vec{e}_r)$$

The one dimensional radial potential gradient is simply

$$en_e\vec{\nabla}\phi = en_e\frac{\partial\phi}{\partial r}\ (+\vec{e_r})$$

Finally, summing over all electron momentum transfer collisions gives the frictional term

$$m_e n_e \sum_i \nu_i(\vec{V_i} - \vec{V_e}) = m_e n_e \sum_i \nu_i(V_i + V_e)\ (+\vec{e_r})$$

Combining the above terms and solving for the potential gradient results in:

$$\frac{\partial\phi}{\partial r} = \frac{m_e V_e}{e}(\frac{\partial V_e}{\partial r} + \frac{2V_e}{r}) + \frac{\partial T_e}{\partial r} + \frac{T_e}{n_e}\frac{\partial n_e}{\partial r} - \frac{m_e}{e}\sum_i \nu_i(V_i + V_e) \qquad (2.3)$$

An expression is needed relating the electron velocity gradient $\frac{\partial V_e}{\partial r}$ to the ionization and recombination rates: S_i, S_r. Defining the electron drift velocity as

$$V_e = -\frac{I_e}{4\pi r^2 e n_e}\ (+\vec{e_r}) \qquad (2.4)$$

where I_e is the electron current crossing a spherical boundary of radius r. The electrons are assumed to be monoenergetic (as are the ions). As a consequence, the corresponding electron and ion drift velocities V_e and V_i are not only the mean species velocity, but also the velocity of the entire population. The electron velocity gradient becomes

$$\frac{\partial V_e}{\partial r} = -[\frac{\frac{\partial I_e}{\partial r}}{4\pi r^2 e n_e} - \frac{2}{r}(\frac{I_e}{4\pi r^2 e n_e}) - \frac{1}{n_e}\frac{\partial n_e}{\partial r}(\frac{I_e}{4\pi r^2 e n_e})] \qquad (2.5)$$

The electron current gradient can be written as a function of the ionization and recombination rates. To accomplish this one recalls that charge conservation requires that the sum of the ion and electron currents remain constant:

$$I_{total} = I_{ion} + I_{electron} = const$$

which implies

$$\frac{\partial I_i}{\partial r} = -\frac{\partial I_e}{\partial r}$$

Defining the ion drift current as

$$I_i = 4\pi e r^2 n_i V_i \tag{2.6}$$

the ion current gradient can be written as

$$\frac{\partial I_i}{\partial r} = (4\pi e)\frac{\partial}{\partial r}(r^2 n_i V_i)$$

The ion continuity equation

$$\frac{1}{r^2}\frac{\partial}{\partial r}(r^2 n_i V_i) = S_i - S_r \tag{2.7}$$

can be used to write the ion current gradient as

$$\frac{\partial I_i}{\partial r} = 4\pi e r^2 (S_i - S_r)$$

and hence the electron current gradient as

$$\frac{\partial I_e}{\partial r} = 4\pi e r^2 (S_r - S_i) \tag{2.8}$$

which is the expression desired. One can now substitute equation (2.4) and equation (2.8) into equation (2.5) to obtain

$$\frac{\partial V_e}{\partial r} = [\frac{S_i - S_r}{n_e} - \frac{2V_e}{r} - \frac{V_e}{n_e}\frac{\partial n_e}{\partial r}]\ (+\vec{e_r}) \tag{2.9}$$

Substituting equation (2.9) into equation (2.3) yields the desired result

$$\frac{\partial \phi}{\partial r} = \frac{m_e V_e}{e}(\frac{S_i - S_r}{n_e} - \frac{V_e}{n_e}\frac{\partial n_e}{\partial r}) + \frac{\partial T_e}{\partial r} + \frac{T_e}{n_e}\frac{\partial n_e}{\partial r} - \frac{m_e}{e}\sum_i \nu_i (V_i + V_e) \tag{2.10}$$

2.2.3 Contactor Ions and Ambient Electrons

To obtain an expression for the contactor ion density, one can expand equation (2.7);

$$\frac{1}{r^2}[r^2(n_i\frac{\partial V_i}{\partial r} + V_i\frac{\partial n_i}{\partial r}) + 2rn_iV_i] = S_i - S_r$$

which yields the following expression for the ion density

$$\frac{\partial n_i}{\partial r} = \frac{S_i - S_r}{V_i} - \frac{n_i}{V_i}\frac{\partial V_i}{\partial r} - \frac{2n_i}{r} \tag{2.11}$$

In this treatment, the contactor ions have been taken to be monoenergetic. The assumption here is that the contactor potential will be much larger than the ion thermal energy. This would have the effect of sharpening the energy distribution, the limiting case being a delta function as assumed here. In this case we can write energy conservation for the ions as

$$\frac{m_iV_{io}^2}{2} + e\phi_o = \frac{m_iV_i^2}{2} + e\phi$$

$$V_i = [\frac{2e}{m_i}(\phi_o - \phi) + V_{io}^2]^{\frac{1}{2}}$$

where ϕ_o and V_{io} are the initial ion potential and velocity respectively. Differentiating this expression one obtains

$$\frac{\partial V_i}{\partial r} = \frac{1}{2}[\frac{2e}{m_i}(\phi_o - \phi) + V_{io}^2]^{-\frac{1}{2}}(-\frac{2e}{m_i}\frac{\partial \phi}{\partial r}) = -\frac{e}{m_iV_i}\frac{\partial \phi}{\partial r} \tag{2.12}$$

Substituting equation (2.12) into equation (2.11) one gets

$$\frac{\partial n_i}{\partial r} = \frac{S_i - S_r}{V_i} - \frac{2n_i}{r} + \frac{en_i}{m_iV_i^2}\frac{\partial \phi}{\partial r} \tag{2.13}$$

The assumption of quasineutrality allows us to relate the electron density gradient $\frac{\partial n_e}{\partial r}$ as contained in equation (2.10) to the ion density in equation (2.13). This can be stated simply as

$$n_e = n_{i_{Ar+}} + n_{i_{O+}}$$

Since the contactor ion density gradient will dominate the ambient oxygen ion density gradient by several orders of magnitude one can write

$$\frac{\partial n_e}{\partial r} \approx \frac{\partial n_{i_{Ar^+}}}{\partial r} = \frac{\partial n_i}{\partial r} \tag{2.14}$$

Equation (2.14) and equation (2.10) can be substituted into equation (2.13) to obtain an expression for the contactor ion density;

$$\frac{\partial n_i}{\partial r} = \frac{\frac{S_i - S_r}{V_i}[1 + \frac{n_i}{n_e}\frac{m_e}{m_i}\frac{V_e}{V_i}] - \frac{2n_i}{r} + \frac{en_i}{m_i V_i^2}\frac{\partial T_e}{\partial r} - \frac{n_i m_e}{m_i V_i^2}\sum_i \nu_i (V_i + V_e)}{[1 - \frac{n_i}{n_e}\frac{1}{m_i V_i^2}(eT_e - m_e V_e^2)]} \tag{2.15}$$

In equation (2.15) it is interesting to note the denominator has approximately a form which is familiar from hydrodynamic theory. This is the familiar sonic point which occurs at the point of minimum area in an ideal one-dimensional channel. In the case of the ion density equation above, there is a critical point when the denominator is zero or

$$\frac{V_e}{V_i} = \sqrt{\frac{(\frac{eT_e}{m_i V_i^2} - \frac{n_e}{n_i})}{m_e/m_i}} \tag{2.16}$$

If at some point in the flow the electron energy (eT_e) is equal to four times the ion kinetic energy ($\frac{1}{2}m_i V_i^2$), the expression above reduces to

$$\frac{V_e}{V_i} \approx \sqrt{\frac{m_i}{m_e}}$$

where for a quasineutral plasma ($\frac{n_e}{n_i} \approx 1$). The presence of such a critical point would seem to suggest the existence of a double solution to this equation, one "subsonic" and one "supersonic". The above expression has the form one would expect for a planar diode where ($n_e \approx n_i$)

$$\frac{j_e}{j_i} \approx \sqrt{\frac{m_i}{m_e}}$$

A more general expression can be obtained by writing equation (2.16) as

$$\frac{j_e}{j_i} = \alpha\sqrt{\frac{m_i}{m_e}} \tag{2.17}$$

where

$$\alpha = \frac{n_e}{n_i}\sqrt{(\frac{eT_e}{m_i V_i^2} - \frac{n_e}{n_i})}$$

Equation (2.17) gives a condition on the ratio of current densities for which the quasineutral assumption cannot be expected to hold since the denominator of equation (2.15) goes to zero. Wei and Wilbur [16] demonstrate that the ratio of currents in a spherical double diode has just the form given by equation (2.17). Such a current ratio would then suggest the existence of a double layer and require a non-quasineutral treatment.

2.2.4 Electron Temperature

An expression for the electron temperature is still required. For this, one can consider the continuity of heat flux Q into a spherical region surrounding the contactor source.

$$\frac{1}{r^2}\frac{\partial}{\partial r}(r^2 Q) = (\frac{I_e}{4\pi r^2})E - 3\frac{m_e}{m_i}n_e e\nu_T(T_e - T_i) - E_{ion}S_i$$

$$\frac{1}{r^2}[2rQ + r^2\frac{\partial Q}{\partial r}] = (\frac{I_e}{4\pi r^2})E - 3\frac{m_e}{m_i}n_e e\nu_T(T_e - T_i) - E_{ion}S_i$$

$$\frac{\partial Q}{\partial r} = (\frac{I_e}{4\pi r^2})E - 3\frac{m_e}{m_i}n_e e\nu_T(T_e - T_i) - E_{ion}S_i - \frac{2Q}{r} \qquad (2.18)$$

In equation (2.18) the first term on the right side represents the ohmic heating in the plasma. The second term reflects the thermal energy exchange between ions and electrons due to elastic collisions. In this term, ν_T represents the total collision rate including turbulence. The third term represents energy exchange through inelastic collisional events and the last term is the geometric fall-off characteristic of a spherical geometry. It is seen from the second term in equation (2.18) that this equation is not exactly consistent with the assumption of a

monoenergetic ion distribution. Again the assumption is that the ion potential energy is much greater than the thermal energy, as well as any change in the thermal energy (proportional to $\frac{m_e}{m_i}$) occurring as a result of elastic collisions with electrons. For the single population of electrons being considered, the first three terms on the right hand side of equation (2.18) are assumed to represent the dominant modes of energy exchange. The electron temperature is related to the heat flux simply as

$$Q = -\kappa \frac{\partial T_e}{\partial r}$$
$$\frac{\partial T_e}{\partial r} = -\frac{Q}{\kappa} \tag{2.19}$$

where the thermal conductivity κ is given by [1]

$$\kappa = \frac{3.2 n_e e T_e}{m_e \nu_T} \tag{2.20}$$

2.3 Anomalous Resistivity

One component of this research was to investigate the sensitivity of contactor performance to turbulent scattering resulting from the presence of instabilities. In this model, two instability modes, ion acoustic and Buneman, were triggered under a prescribed set of condition. A simple expression for the ion acoustic instability-driven collisions is given by

$$\nu_{ion-acoustic} = 10^{-2} \frac{T_e}{T_i} \frac{v_D}{v_{ther}} \omega_{pe} \tag{2.21}$$

where v_D is the differential drift velocity between the ions and electrons, and ω_{pe} the plasma frequency. This instability is triggered if the drift velocity exceeds a critical velocity defined by [12]

$$v_{crit} = c_s/\sqrt{2}(1 + \sqrt{T_e m_i/(m_e T_i)}(T_e/T_i) \exp(-\frac{3}{2} - \frac{1}{2}\frac{T_e}{T_i}))$$

If one considers a simplified form of the electron momentum equation, it is possible to define an electric field such that the electrons drift at a constant velocity, the force of the electric field being counteracted by the retarding force of collisions. The expression for such an electric field is given by

$$E = \frac{m_e}{e}\nu_e v_D$$

If the relative ion-electron drift velocity v_D is less than the electron thermal velocity, then the frictional term in the momentum balance will increase with drift velocity ($\nu_T m_e v_D \sim v_D/v_{th}^3$). However, if the drift velocity is greater than the thermal velocity, the frictional term will decrease with increasing drift velocity ($\nu_T m_e v_D \sim 1/v_D^2$). From this it is apparent that if the drift velocity exceeds the thermal velocity, the frictional term will only decrease and the drift velocity continue to increase. The electric field which insures $v_D = v_{th}$ is known as the Dreicer electric field. Setting the drift velocity equal to the thermal velocity in the equation above one obtains

$$E_{Dreicer} = \frac{m_e}{e}\nu_e v_{the}$$

Exceeding this electric field, or alternatively, $v_D > v_{th}$ triggers an instability known as the Buneman instability, the collision frequency given approximately as [7]

$$\nu_{Buneman} = 0.53(\frac{m_e}{m_i})^{0.61}\omega_{pe} \tag{2.22}$$

In the above relations, the drift velocity v_D is defined in terms of the total current as

$$v_D = \frac{I}{4\pi r^2 e n_e}$$

which can be written in terms of the ion and electron velocities as

$$v_D = V_e + V_i\frac{n_i}{n_e}$$

2.4 Non-Dimensional Equations

2.4.1 Characteristic Values

In order to facilitate the numerical solution of the governing equations it was useful to rewrite them in non-dimensional form. Characteristic values used in the non-dimensionalization are denoted by a zero subscript and are defined as follows.

Velocity

$$V_0 = c_s$$

where c_s is the ion accoustic velocity defined as

$$c_s = [\frac{2eT_e}{m_i}]^{\frac{1}{2}}$$

Radius

$$r_0 = \lambda_D$$

where λ_D is the Debye length

$$\lambda_D = [\frac{\varepsilon_o T_e}{n_e e}]^{\frac{1}{2}}$$

Density

$$n_0 = n_{amb}$$

Potential

$$\phi_0 = T_{e_{amb}}$$

where $T_{e_{amb}}$ is the ambient electron temperature in eV.

Temperature

$$T_0 = T_{e_{amb}}$$

Rate of Density Change

$$S_0 = \frac{c_s n_{amb}}{\lambda_D}$$

Current

$$I_0 = I_i \mid_{r_o}$$

where $I_i \mid_{r_o}$ is the ion current emitted from the contactor.

Electric Field

$$E_0 = \frac{\phi_0}{\lambda_D}$$

Heat Flux

$$Q_0 = (\frac{I_i \mid_{r_o}}{4\pi r_o^2}) T_e \mid_{r_o}$$

In the expression above, Q_0 represents the electron heat flux out of the sphere of initial radius r_o.

In addition to the expressions listed above, it is also convenient to define the following characteristic energies which enable further simplification of the equations when written in non-dimensional form.

$$E_e^* = m_e c_s^2$$

$$E_i^* = m_i c_s^2$$

$$T^* = eT_0$$

$$P^* = e\phi_0$$

It is also convenient to define a characteristic drift velocity V_D^* as

$$V_D^* = \frac{I_i \mid_{r_o}}{4\pi\lambda_D^2 e n_{amb}}$$

2.4.2 Non-Dimensionalized Equations

If we denote non-dimensional variables by a "~" we can write out the previously derived governing equations in non-dimensional form. The set of equations for the quasineutral solution become

$$\frac{\partial \tilde{n}_n}{\partial \tilde{r}} = \frac{\tilde{S}_r - \tilde{S}_i}{\tilde{V}_n} - \frac{2\tilde{n}_n}{\tilde{r}} \tag{2.23}$$

and

$$\frac{\partial \tilde{n}_i}{\partial \tilde{r}} = \frac{(\tilde{S}_i - \tilde{S}_r)[\frac{1}{\tilde{V}_i} + \alpha V_e] - \frac{2\tilde{n}_i}{\tilde{r}} + \alpha \frac{T^* \tilde{n}_e}{E_e^*} \frac{\partial \tilde{T}_e}{\partial \tilde{r}} - \alpha \tilde{n}_e \sum_i \nu_i (\tilde{V}_i + \tilde{V}_e)(\frac{\lambda_D}{C_e})}{1 - \alpha[\tilde{T}_e(\frac{T^*}{E_e^*}) - \tilde{V}_e^{\,2}]} \tag{2.24}$$

where

$$\alpha = \frac{1}{\tilde{V}_i^{\,2}} (\frac{\tilde{n}_i}{\tilde{n}_e}) \frac{E_e^*}{E_i^*}$$

$$\frac{\partial \tilde{\phi}}{\partial \tilde{r}} = \frac{(\tilde{S}_i - \tilde{S}_r)}{\tilde{n}_e} \tilde{V}_e (\frac{E_e^*}{P^*}) + \frac{1}{\tilde{n}_e} \frac{\partial \tilde{n}_e}{\partial \tilde{n}_r} [\tilde{T}_e (\frac{T^*}{E_e^*}) - \tilde{V}_e^{\,2}] (\frac{E_e^*}{P^*}) + \frac{\partial \tilde{T}_e}{\partial \tilde{r}} (\frac{T^*}{P^*}) - \sum_i \nu_i (\tilde{V}_i + \tilde{V}_e)(\frac{E_e^*}{P^*})(\frac{\lambda_D}{c_s}) \tag{2.25}$$

$$\frac{\partial \tilde{Q}}{\partial \tilde{r}} = \frac{\tilde{I}_e}{\tilde{r}^2} \tilde{E} (\frac{V_D^* P^* n_{amb}}{Q_0}) - 3\tilde{n}_e \nu_T (\tilde{T}_e - \tilde{T}_i)(\frac{m_e}{m_i} \frac{n_{amb} T^* \lambda_D}{Q_0}) - \tilde{S}_i (\frac{E_{ion} c_s n_{amb}}{Q_0}) - \frac{2\tilde{Q}}{\tilde{r}} \tag{2.26}$$

$$\frac{\partial \tilde{T}_e}{\partial \tilde{r}} = -\tilde{Q} (\frac{Q_0 \lambda_D}{T_{amb} \kappa}) \tag{2.27}$$

$$\frac{\partial \tilde{n}_e}{\partial \tilde{r}} = \frac{\partial \tilde{n}_i}{\partial \tilde{r}} \tag{2.28}$$

2.5 Numerical Solution

The one-dimensional, normalized equations were solved using a package called LSODE which solves a system of first order differential equations. This package is based on the GEAR and GEARB packages and is designed to handle both stiff and non-stiff problems using either an internally generated or user supplied Jacobian matrix. LSODE is an initial value problem solver. As a result it was necessary to specify initial conditions for the dependent variables at the contactor. Since the potential is determined relative to the ambient plasma, the value for ϕ was taken as zero at r_o and a potential drop determined at the core boundary.

Physically, the electron current entering the core cloud at its boundaries cannot exceed that obtained from the random electron flux into the cloud. Since the size of the core cloud was not known, an iterative solution was required. This was done by selecting a contactor ion current and guessing the collected electron current. LSODE would then integrate the previous equations until the core boundary condition was satisfied. At this point the random thermal current into the cloud was evaluated and the total current compared with the initial guess. A bisection algorithm was incorporated and convergence on the solution was obtained usually in less than ten iterations.

Chapter 3
Sensitivity of Contactor Performance

3.1 Introduction

This chapter discusses the results of a parametric study to assess the performance of a plasma contactor under a wide range of operating conditions. Two figures of merit from a space systems standpoint are the current collection capability and the efficiency of the contactor device. The first of these will be quantified by means of the electron current gain (ξ) defined simply as

$$\xi = \frac{I_{ion} + I_{elec}}{I_{ion}} = \frac{I}{I_c}$$

where I_{ion} and I_{elec} represent the ion and electron currents at the contactor radius r_o. The efficiency η is inversely proportional to the potential drop $\Delta\Phi$ sustained across the core region of the plasma cloud associated with the anode and cathode, i.e.

$$\eta \approx \frac{V_L}{V_L + \Delta V_a + \Delta V_c}$$

In addition to the gain and efficiency, we seek to determine the size of the one-dimensional cloud core as determined by the two models previously discussed. These three features will serve then to grossly define the contactor's performance.

To assess the variation of contactor performance under under various conditions it was necessary to examine factors which could be controlled either

by component design or choice of operating conditions as well as those which depend directly upon the operating environment and hence cannot be directly controlled. Four parameters were chosen to map out contactor performance in this study; these were:

- I_c Contactor Ion Current
- n_{amb} Ambient Ion Density
- $T_e|_{r_o}$ Electron Temperature at Contactor
- M_o Initial Contactor Ion Mach No.

Of these four variables, really only the current I_c and the injection mach number M_o can be directly controlled. The ambient oxygen ion density n_{amb} is dependent on the the altitude of the orbit as well the incidence of solar radiation. The electrons present in the vicinity of the contactor are primarily those from the far-field which have drifted towards the positively biased contactor. In some cases there may be additional electrons as a result of ionization within the core cloud. In general however, the electron temperature and hence the heat flux in this region cannot be directly controlled. However the temperature will affect the degree to which ionization can occur and hence impacts the ability of the contactor to enhance current flow. For this reason, the influence of high and low temperature electrons at the contactor was studied as well. In all the results which follow, unless stated otherwise, the set of default parameters is as follows: electron temperature $T_e = 0.5eV$, initial contactor plasma ionization fraction $f_i = 10^{-1}$, contactor ion current $I_c = 1A$, ambient oxygen ion density $n_{amb} = 2 \times 10^{12} m^{-3}$, initial radius of core cloud $r_o = 0.1m$, ion injection mach number (relative to ion acoustic speed) $M_o = 1.0$.

3.2 Relation of the Core Definition to Performance Curves

The core cloud in this model represents a collisional region where the plasma expansion is assumed to be one-dimensional. In large part, the gain and potential drops are directly related to the size of this cloud. As has been discussed, two different criteria were used to define the outer boundary of this cloud. The E/vB condition represents a ratio of electron radial drift to induced $\vec{v_e} \times \vec{B}$ drift and as such constitutes a macroscopic criteria. The collisionality or ν/ω condition on the other hand reflects the degree to which the electrons are magnetized and constitute a microscopic criteria. Much of the results presented here can be understood by recognizing some important features of the core defining criteria.

The collisionality condition is defined as the ratio of collision frequency for the electron to the corresponding gyrofrequency. The collision frequency includes classical as well as Buneman and ion acoustic turbulent collisions. The electron gyrofrequency will be a function of the diamagnetically modified magnetic field and is given by

$$\omega = \frac{eB}{m_e}\sqrt{1-\beta} \quad \beta < 1$$

$$\omega = 0 \quad \beta \geq 1$$

In these expressions, the beta parameter (β) is defined as the ratio of plasma pressure to magnetic pressure and is given by:

$$\beta = \frac{\sum_i n_i e T_i}{B^2/2\mu_o}$$

where the sum is over all the species present. The collisionality stopping condition must always reach a value of one outside of the core region defined by

beta equal to unity. While the beta parameter will decrease rapidly, close to the contactor where the electron density and temperature is changing rapidly its variation is slow beyond the point where beta equals one. Beyond this point it approaches a final value asymptotically as the densities and temperatures approach their ambient values. Hence, while the diamagnetically modified magnetic field is not constant, its variation is not significant beyond the point where beta has reached a value of unity. As a consequence, the collisionality stopping condition ($\nu/\omega \propto \nu_T/B\sqrt{1-\beta}$) decreases primarily because the electron collision frequency is decreasing. For this reason, curves which represent the collisionality stopping condition can in many cases be understood on the basis of what effect the particular parameter which is being mapped out has upon the collision frequency. Understanding how the collision frequency in turn affects a particular performance parameter such as core radius, gain, or potential drop then leads to a relatively simple picture of what underlying processes are occurring.

For the case of the E/vB core criteria the situation is less clear. This is due to the fact that a larger number of dependent variables are involved in the expression for the electric field and electron velocity so that it becomes much more difficult to establish a direct relationship to any one in particular. In the general case, the electric field is given by the electron momentum equation (2.10) which depends upon temperature and density gradients, collision frequencies, and ionization rates. For the majority of operating conditions considered, the dominant terms in this equation were the density gradient and collisional terms. If one considers the behavior of only these terms, it is possible to understand the general trends which were observed; however some particular features such as local extrema require consideration of other terms as well.

It is important to keep in mind that each point in each curve presented in this section represents the results of an integration over a cloud radius for a particular set of conditions. Some effects are pronounced for only a very short distance away from the contactor and, as a consequence, their effects are not always evident in these curves which represent results integrated in some cases over tens of meters. An example of such an effect is the ionization associated with high electron temperatures and ion densities. While high electron temperatures (tens of eV) lead to high ionization rates, the temperatures fall off quickly as does the ion density. As a consequence, the effect of the high ionization is only seen over a very short distance.

3.3 Core Cloud Radius

3.3.1 Variation of Core Radius with Ion Current

Figure 3.1 shows the one dimensional core cloud radius plotted as a function of the logarithm of the ion current. The core corresponding to the E/vB stopping condition is seen to range in size from about 0.9m at 10mA to 3.3m at 1A. The curve corresponding to the collisionality condition ranges from 0.125m to 0.72m for the high and low currents respectively. As will be seen in all of the core radius curves in this section, the collisionality condition predicts a smaller core which is consistent with the earlier discussion of boundary criteria.

It is evident from Figure 3.1 that for both boundary conditions the core radius increases with ion current. For the E/vB curve this can be understood from an examination of the electron momentum equation. From the simplified

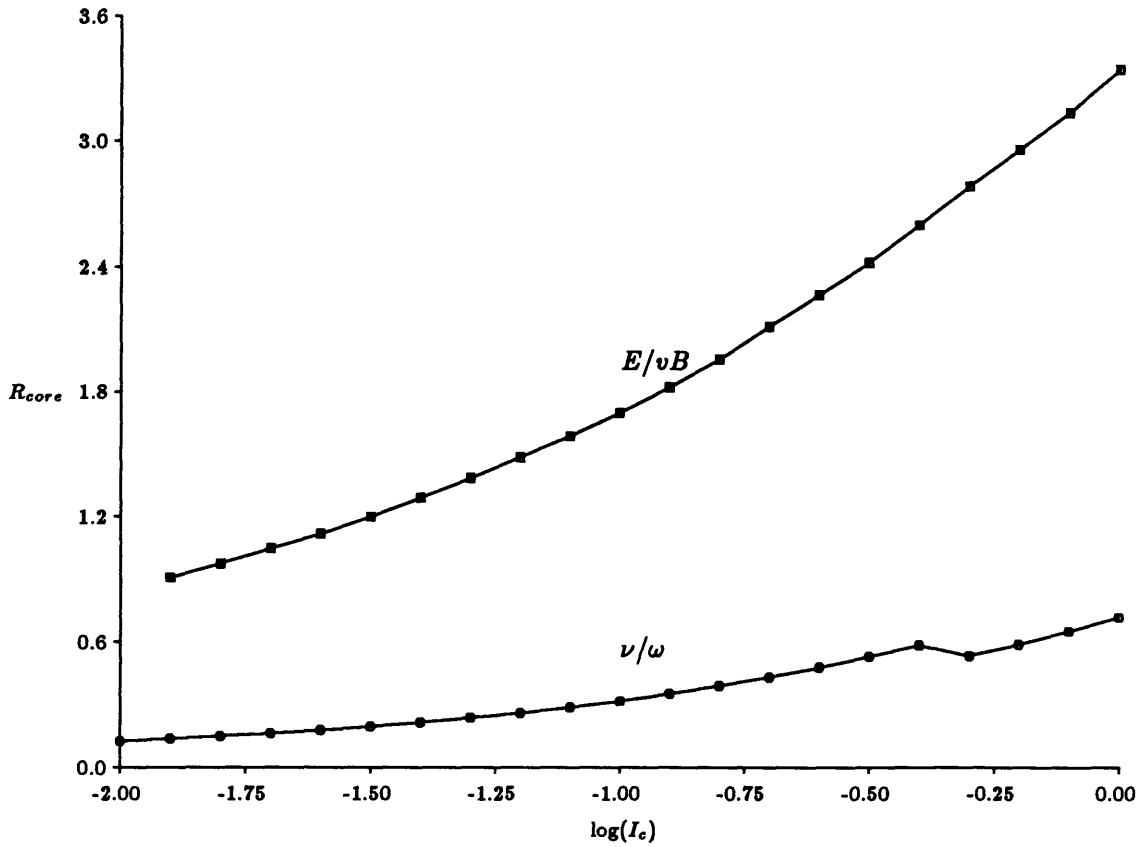

Figure 3.1: Core Radius vs. Log of Ion Current

electron momentum equation (2.1) it is evident that the initial electric field, and hence the initial value of E/vB is proportional to the electron density gradient. Because quasineutrality has been imposed, this gradient is equal to the ion density gradient given by equation (2.15). From this equation it can be seen that the density gradient will increase with initial ion density or current since the injection velocity is fixed.

The value of E/vB always varies from some number larger than one to one.

The increasing core radius for the E/vB condition is hence a direct consequence of the larger initial electric field. Some additional insight can be gained if one considers the core radius, and potential drop curves as well, from the standpoint of a system behaving as a classically resistive medium in which the potential increases with both the current and resistivity.

In this formulation the contactor potential was not an independent variable but rather was equal to electric field integrated from some initial value E_i (given by equation (2.10)) to the point where E_f was equal to vB. Mathematically, one can consider the cloud potential drop to be the area enclosed under a plot of the electric field versus radius from r_o to $r_c|_{E=vB}$. Since the shape of these curves $\frac{\partial E}{\partial r}$ is not a strong function of ion current, the larger initial values of electric field enclose a larger area , indicating a larger potential drop. Physically, the electric field must fall to zero in the far field since there is no mechanism (at least included in this model) which would allow it to do otherwise. Increasing the initial electric field steepens the potential well into which the ions can fall. Ions falling into a deeper well travel a larger distance radially before reaching the bottom, resulting in a larger core.

For the collisionality condition the radius also increases with ion current although at a somewhat smaller rate. Increasing ion current at constant injection velocity results in a corresponding increase in ion, electron and neutral particle densities. The collision frequencies increase with particle density and will therefore increase as well. As mentioned previously, the collisionality parameter ν/ω is essentially a non-dimensional collision frequency since the gyrofrequency does not vary greatly beyond the point where beta is equal to unity. As a consequence, the collisionality curve merely reflects the fact the collisions are

increasing with ion current.

The fact the E/vB curve increases at a faster rate than the collisionality curve can be understood by recognizing that the collisionality curve depicts the increase in resistivity with current. The E/vB curve, on the other hand, represents the increase in potential with current which increases faster since it is the product of two increasing numbers, the current and resistivity.

Finally there is a small kink in the collisionalty curve at roughly 0.4A. This is due to an increase in the collision frequency which results from the Buneman collision term being triggered. This term increases the collision frequency by roughly $10^5 sec^{-1}$.

3.3.2 Variation of Core Radius with Ambient Density

Figure 3.2 shows the core radius plotted against the logarithm of ambient ion density for values ranging from $10^9 m^{-3}$ to $10^{13} m^{-3}$. This range is expected to cover the extremes one might expect over night and day cycles in the ionosphere year round. For the E/vB stopping condition, the radius is seen to range from 39.7m at the lowest density decreasing to 1.9m at the highest. The core defined by the collisionality condition is seen to be insensitive to variations in ambient ion density having a constant value of 0.717m.

For the self-consistent solution the electron current collected is proportional to the square of the core radius times the ambient density.

$$I_e \propto r_c^2 \cdot n_{amb}$$

The electron currents collected varied from 88mA at an ambient density of

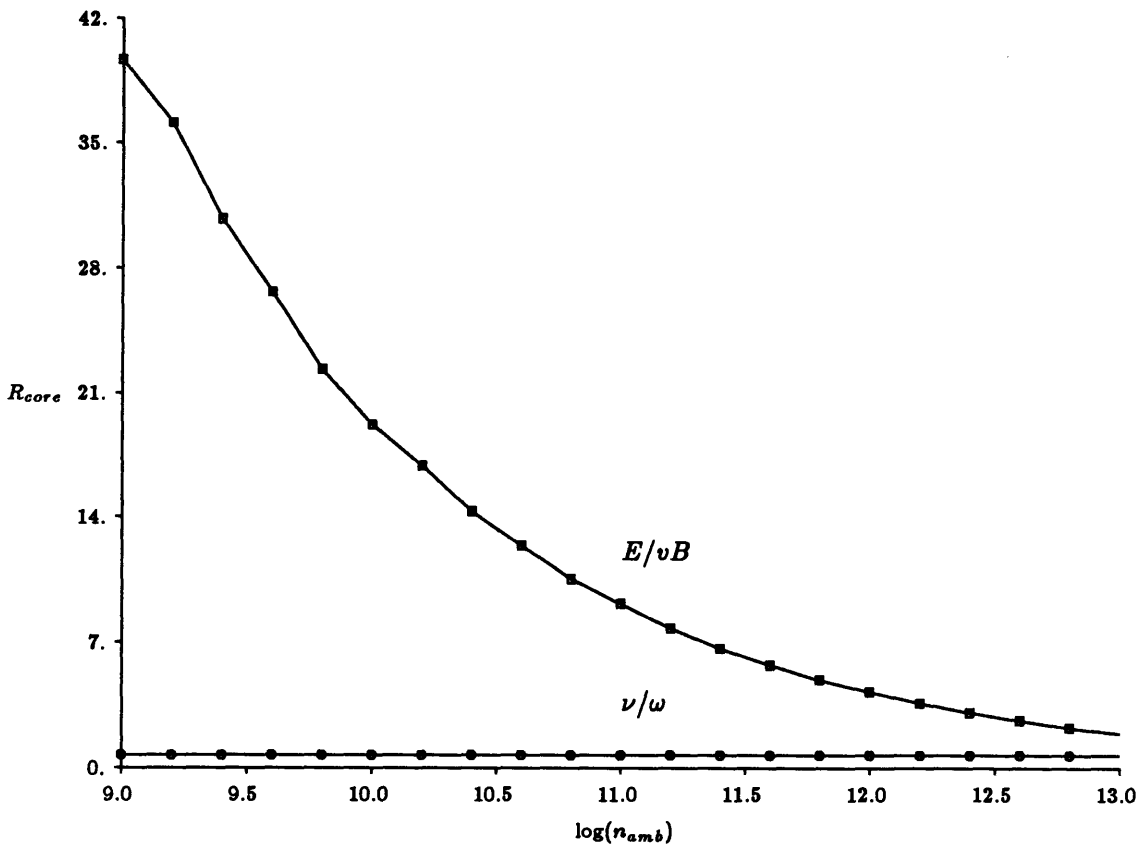

Figure 3.2: Core Radius vs. Log of Ambient Ion Density

$10^9 m^{-3}$ to 1.95A at an ambient density of $10^{13} m^{-3}$. This represents an increase by a factor of 22.2. Since the ambient density increases by four orders of magnitude, the simple proportionality given above would require the collection area to decrease by a factor of 427, and the core radius by a factor of 20.6. This is, in fact, the decrease in core radius observed in Figure 3.2.

The above argument reflects only the manner in which the cloud size scales with electron current and ambient density. The more fundamental question is

what determines the variation observed in the electron current. One can well ask, what are the independent parameters determining the electron current? The ambient density is independent and treated as such in the formulation of the problem. This is reasonable since it will be determined by conditions in the ionosphere which exist during the time the contactor is operating. The question is then how are the electron current and core radius related? Since ionization does not play a significant role for the given range of currents and electron temperatures, the electron current collected will be that due to the far field. It will be seen in Figure 3.10 that the electron current increases with ambient density. Furthermore, from Figure 3.2 one sees the core radius is decreasing with increasing ambient density (and hence electron current as well). In Figure 3.1 the core radius was seen to increase with ion current. From this we conclude the core radius for the E/vB condition will increase with ion current and decrease with electron current. The reason for this is seen in in the denominator of equation (2.15). Quasineutrality requires the electron density equal the ion density. As electron current increases and ion current remains fixed, the electron velocity will increase (as required by continuity) resulting in the magnitude of the ion (and electron) density gradient decreasing since the denominator in equation (2.15) must increase. The result of this as evident in the electron momentum equation (2.1) is a lower initial electric field and hence a smaller core. Increasing ion current results in a higher ion density (since the injection velocity is fixed) and as a consequence initial electric field increases along with the density gradient.

In Figure 3.2 the ion current is fixed and the electron current is increasing, the result is a decreasing core radius as just discussed. For any given point on this curve, the electron current and core radius will be those required by the consistency condition and the proportionality discused earlier.

While it is true that the total collision frequency increases with ambient ion density, for the cases considered the ambient ion density was always much less than the contactor ion density. As an example, at $I_c = 1.0A$ and $r_o = 0.1m$, the contactor ion density is on the order of $10^{15}m^{-3}$ when injected at the ion acoustic speed. This density is still several orders of magnitude larger than ambient ion density for most of the cases considered. The dominant collision frequencies are then the electron-contactor ion and electron-contactor neutral which are virtually insensitive to the ambient density. This insensitivity is reflected in the collisionality curve which does not vary with the ambient density.

3.3.3 Variation of Core Radius with Initial Electron Temperature

Figure 3.3 shows the variation of core radius with initial electron temperature for temperatures ranging from 0.5eV to 10.0eV. The curve corresponding to the E/vB boundary condition varies from a value of 3.84m at 0.5eV to 3.94m at 6.7eV. This curve does not extend over the full range of temperatures since for cases above 6.7eV the ambient ion density was reached before the stopping condition could be met. The curve corresponding to the collisionality condition shows a somewhat larger variation ranging from 0.717m at 0.5eV to 2.63m at 10.0eV.

The curves corresponding to both stopping conditions show a general increase with electron temperature although this increase is not monotonic. In particular the curve corresponding to the E/vB condition shows a local maxima at approximately 1.9eV. An examination of the electron-ion collision frequencies

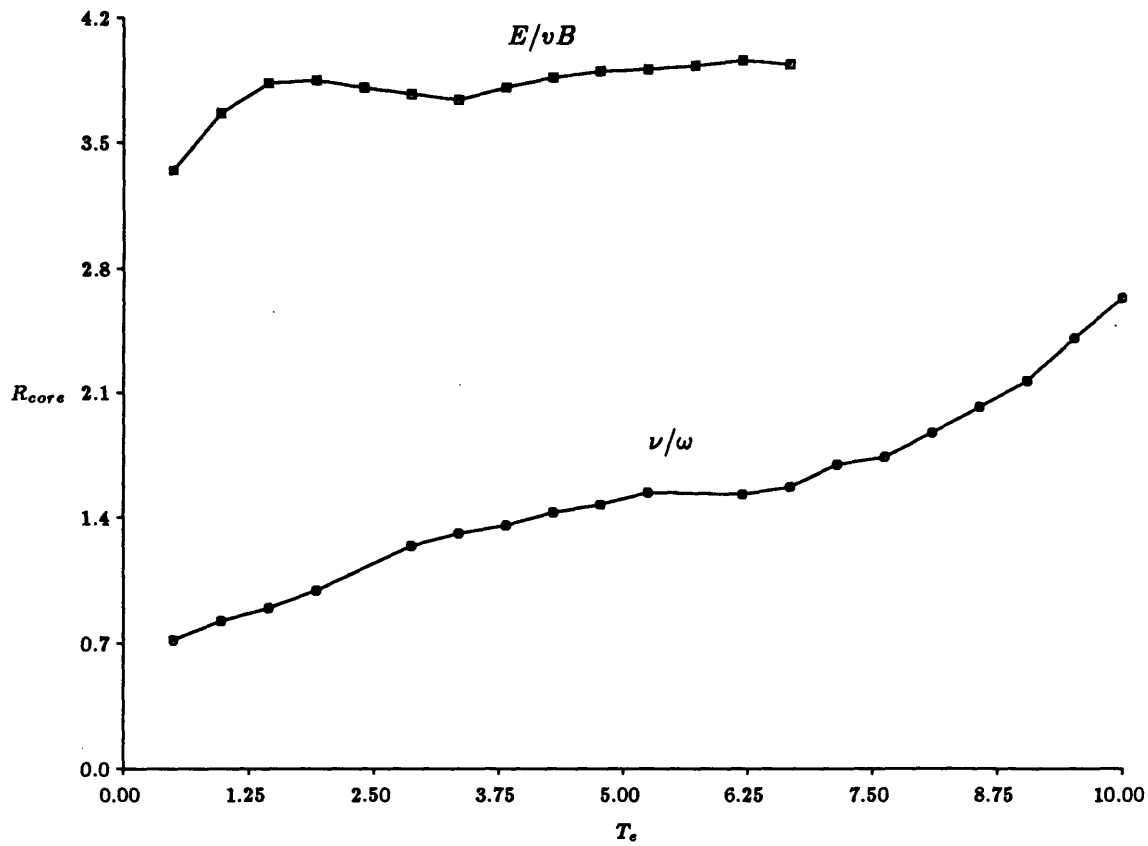

Figure 3.3: Core Radius vs. Initial Electron Temperature

for both contactor and ambient neutrals reveal that these collision frequencies increase with increasing electron temperature. That is, they have the form

$$\nu_{e-i} = C \cdot n_i \cdot T_e^{-\frac{3}{2}} \cdot (B - \log(\sqrt{\frac{n_e}{T_e}}))$$

where C and B are constants, n_i and n_e are the ion and electron number densities and T_e is the electron temperature. The increase in collision frequency results in a correspondingly larger core for the collisionality defined cloud since for this

boundary condition the cloud size is a direct measure of the collision rate.

For the E/vB curve the relation is not as obvious. It is helpful to recall the simplified form of the electron momentum equation used earlier to show the relation of the two stopping conditions.

$$\frac{E}{v_e B} = \frac{\nu_e}{\omega} - \frac{T_e}{e n_e v_e B}\frac{\partial n_e}{\partial r} + \frac{1}{\omega v_e}(\nu_{ei} v_i + \nu_{en} v_n)$$

Since the ion density is always decreasing, the second term in the above equation is positive. Increasing the electron temperature is then seen to increase the electric field since each term in the above equation will increase. The reason for the local maxima and varying slope evident in the E/vB curve is not immediately obvious. However, the cause of these fluctuations is likely to rest in the second term in the above equation, specifically the ion density gradient (equal to the electron density gradient for a quasineutral plasma). Examination of equation (2.15), the ion density gradient, reveals that the gradient is a nonlinear function of the electron temperature which itself is changing. The conclusion is that while the ion density always decreases, the rate of decrease will vary with electron temperature in some complicated way resulting in the fluctuations and local extrema seen in Figure 3.3.

3.3.4 Variation of Core Radius with Injection Mach No.

Figure 3.4 shows the cloud radius as a function of contactor ion injection mach number. This is the mach number based on the ion acoustic velocity. The mach number parameter space spanned a range from 0.5 to 10. For the E/vB curve the calculated values of the core radius are seen to decrease from 3.32m

at the lowest mach number to 2.28m at the highest mach number. For the case of the core defined by the collisionality condition, the size of the cloud is also seen to decrease this time from 0.718m at $M_o = 0.5$ to 0.438m at $M_o = 10$. Interesting features of these curves include a local maxima for the E/vB curve at roughly $M_o = 0.7$ and a kink in the collisionality curve at about $M_o = 5$.

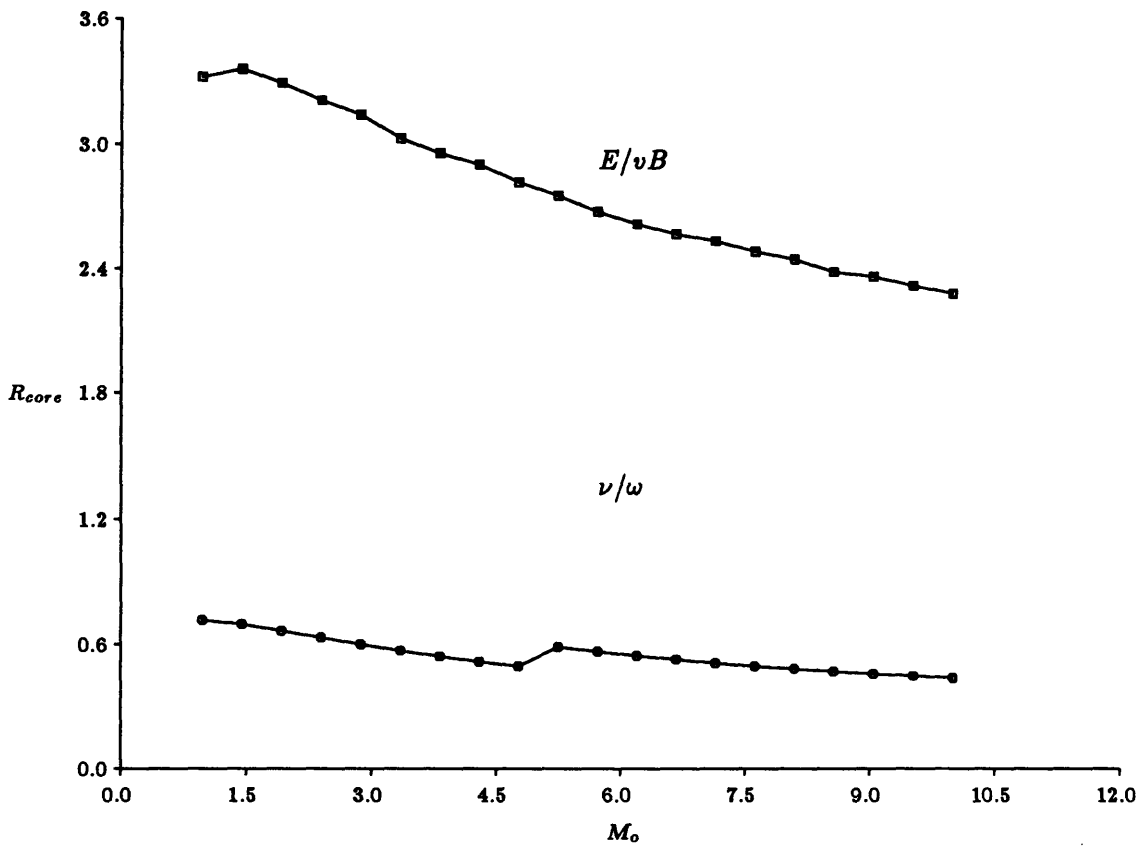

Figure 3.4: Core Radius vs. Injection Mach No.

The general decreasing trend evident in both of the curves is easily understood. For a given ion current, increasing the injection velocity as the effect of

lowering the initial ion density since the current density is fixed. Lowering the density has an overall effect similar to lowering the current since for that case the initial current density decreased while the injection speed was fixed. The net result is a lowering of the total collision frequency resulting in smaller radii for both boundary conditions as discussed previously.

The exact reason for the location of the local maxima in the E/vB curve is not easily pinpointed. However the general behavior can be understood on the basis of arguments already made for the case of Figure 3.3. In particular, the ion density gradient is a nonlinear function of the ion velocity. For a given set of conditions, the ion density will not always decrease at the same rate. For this reason the second term in the simplified momentum equation shown above will change in magnitude leading to a situation as seen in Figure 3.4 where two different mach numbers can result in the same core radius.

The kink seen in the collisionality curve is a consequence of the Buneman collision term triggering. As the ion velocity increases, so does the differential ion-electron drift velocity. Eventually this velocity exceeds the critical velocity which triggers the Buneman collisions.

For the operating conditions considered in this study the one-dimensional core radius has been seen to vary from roughly a meter up to tens of meters for the E/vB core condition. The collisionality stopping condition consistently predicted smaller clouds with radii ranging generally up to a few meters.

To date, terrestrial laboratory experiments have been limited to investigation of a region on the order of a meter radius surrounding the hollow cathode plasma source. On such a scale it is not expected that such experiments would be

able to reproduce the current enhancement which occurs as a consequence of collecting far field electrons over a significantly larger effective collection area tens of meters in diameter. On the other hand, and perhaps more importantly, the larger vacuum tanks should be sufficiently large to enable investigation of the region where the steepest potential and density gradients occur, namely within two or three meters of the source.

3.4 Core Potential

3.4.1 Variation of Potential Drop with Ion Current

Figure 3.5 shows the cloud potential drop as a function of the logarithm of the contactor ion current. The curve corresponding to the E/vB stopping condition is seen to increase from 2.3V at 10mA to 3.6V at 1.0A. The core defined by the collisionality condition also increases with ion current. This curve ranges from 0.35V at the low current to 2.5V at the high current.

The curve corresponding to the collisionality stopping condition is seen to be linear, implying an exponential dependence of cloud potential with contactor ion current. Again this can be understood from the fact that the plasma is behaving as a classically resistive medium. The exponential dependence results from the fact the resistivity increases with the current.

The curve for the E/vB stopping condition also shows the expected increase in potential with ion current. One difference is in the general flattening of the top curve and the appearance that it might approach some asymptotic value.

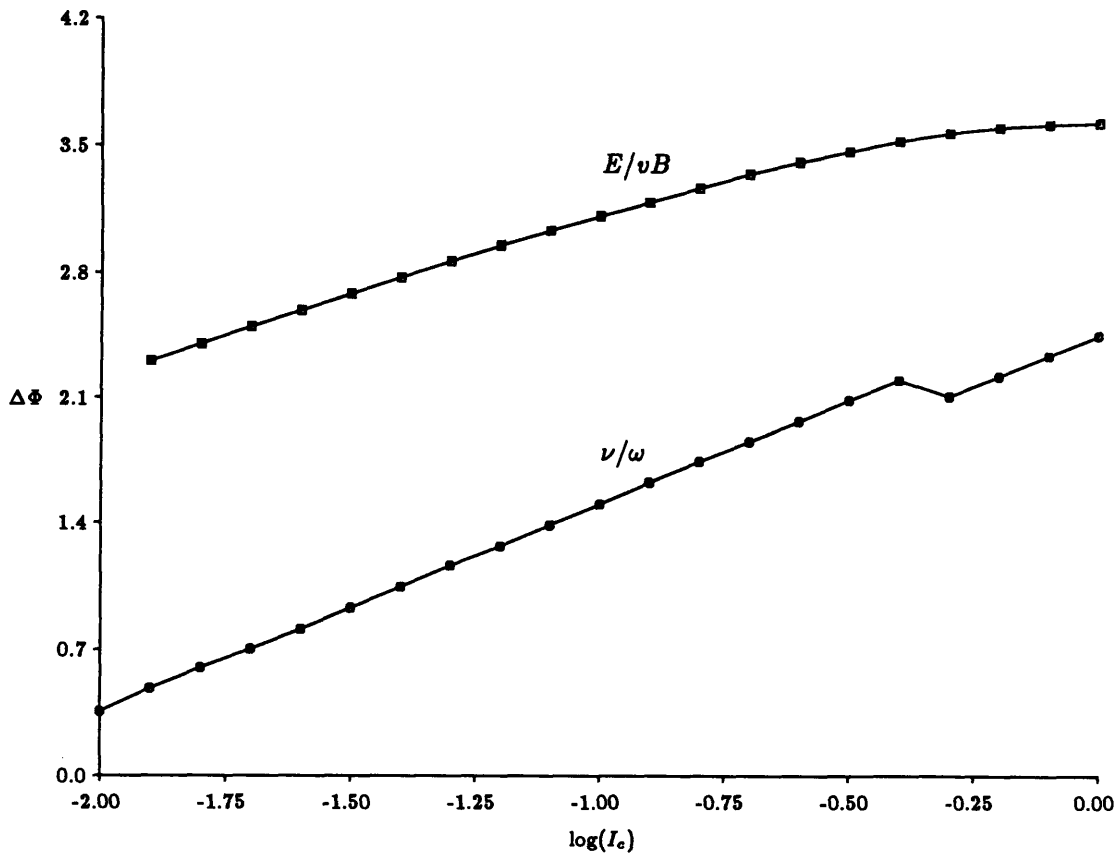

Figure 3.5: Potential Drop vs. Log of Ion Current

From examination of the electric field profiles for individual cases it was evident that most of the potential drop occurs in roughly the first meter of the cloud. Beyond this the potential profile becomes much more shallow and while the electric field may not fall low enough to reach the core condition for several more meters, the contribution of this remaining region to the total potential drop is small by comparison to that which occurs in the first meter or two.

If one examines Figure 3.5 it is seen that the maximum core radius attained

by the collisionality curve, and the minimum attained by the E/vB curve, is roughly 0.8m. From Figure 3.1 it is evident that the potential associated with both curves at this radius is approximately 2V. Shifting the E/vB curve down by this amount then gives an indication of the potential drop due to the cloud beyon a radius of 0.8m. The potential drop only increases by just over one volt even though the radius of the cloud increases up to three meters. The fact the E/vB curve is non-linear at the high end is because its cloud has had a chance to get to a radius large enough where the electric field has become very small. This is why the potential curve in Figure 3.5 in flattening even though the core in Figure 3.1 is increasing.

The collisionality curve is linear because it is always within the first meter of the core where the electric field is still substantial. From inspection of the E/vB curves in Figures 3.1 and 3.5, it is evident the potential drop is linear with the logarithm of ion current for radii below about 2.5m.

The kink in the collisionality curve is again due to the onset of the Buneman collisions (the same kink observed in Figure 3.1).

3.4.2 Variation of Potential Drop with Ambient Density

Figure 3.6 shows the variation of potential drop with the logarithm of the ambient ion density. The curve corresponding to the E/vB stopping condition is seen to decrease with increasing ambient density from a value of 6.3V at an ambient density of $10^9 m^{-3}$ to 3.0V at a density of $10^{13} m^{-3}$. The collisionality curve is virtually insensitive to the ambient density with a potential drop of only 2.4 V over the entire range considered.

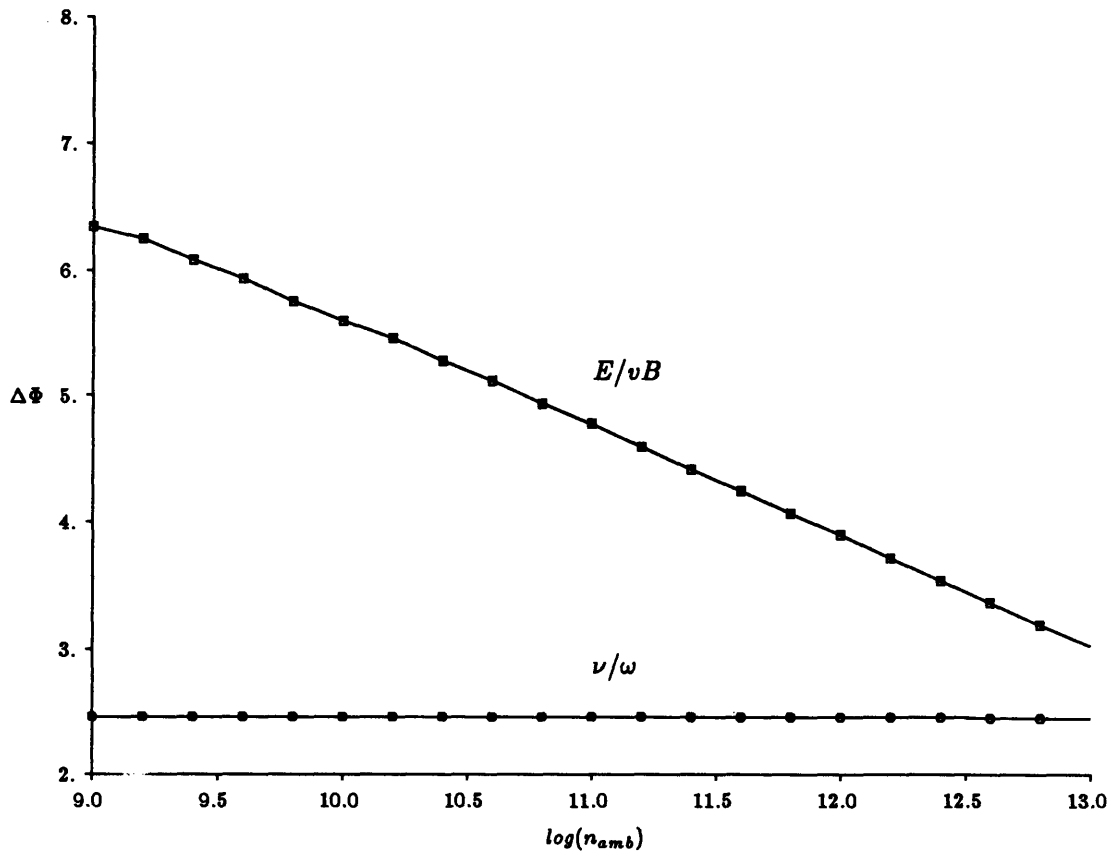

Figure 3.6: Potential Drop vs. Log of Ambient Ion Density

The potential drop for the E/vB curve decreases with increasing ambient density as did the core radius curve although at a substantially lower rate. In fact it only decreases by roughly a factor of two. The fact it is decreasing is consistent with fact the core size is decreasing as well. As discussed previously, this is a consequence of the fact the initial electric field is decreasing and hence requiring a shorter distance to reach the stopping condition. While the initial electric field does not directly have information on the ambient density, this information is conveyed through the electron current which is determined iteratively as the

program seeks the self consistent solution. Determination of the self consistent solution does in fact incorporate information about the ambient density since the electron current at the core radius has to be bounded by the random electron flux into the cloud.

As was seen with the case of core radius vs. ambient density (Figure 3.2) the collisionality stopping condition is virtually insensitive to changes in the ambient density. Since even large changes in the ambient ion density result in only small changes in the electron density, the result is virtually no change in either the collision frequencies or the electric field.

3.4.3 Variation of Potential Drop with Initial Electron Temperature

The variation of potential drop with respect to initial electron temperature is shown in Figure 3.7. Both curves increase almost linearly with electron temperature. The top curve corresponding to the E/vB stopping condition ranges from 3.63V at 0.5eV to 44.5V at 6.7eV. This curve does not extend the full range of temperatures since the ambient density was reached before the stopping condition could be satisfied for temperatures above 6.7eV. The curve corresponding to the collisionality stopping condition ranges from 2.45V at 0.5eV to 69.3V at 10.0eV.

Referring back to the simplified form of the electron momentum equation discussed earlier it is evident that the initial electric field is a strong function of the initial electron temperature. In addition the largest percentage of the potential drop will occur in the first meter or so of the cloud where the electric

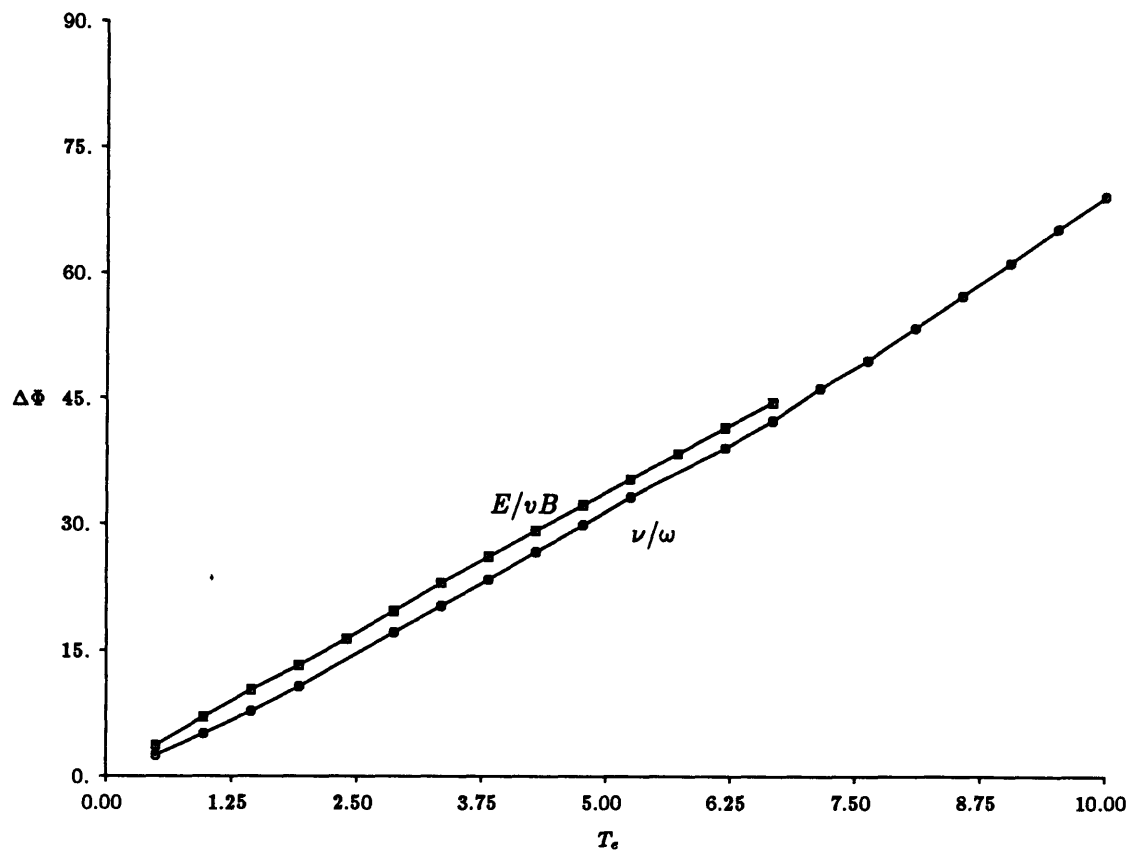

Figure 3.7: Potential Drop vs. Initial Electron Temperature

field is strongest. These two observations are consistent with Figure 3.7 where the potential is seen to be a strong linear function of the electron temperature even though the corresponding core radii (in Figure 3.3) do not vary a great deal. For the currents considered (less than 1.0A) the effect of ionization was not found to be significant even at 10.0eV.

3.4.4 Variation of Potential Drop with Injection Mach No.

Figure 3.8 shows the variation of core potential drop as a function contactor ion injection mach number. The curve corresponding to the E/vB stopping condition decreases slightly from 3.62V at $M_o = 0.5$ to 2.99V at $M_o = 10$. Over the same range of mach numbers, the potential drop associated with the collisionality stopping condition decreases from 2.47V to 1.55V.

As was mentioned in the discussion of Figure 3.4, the effect of increasing the injection velocity at constant current is to decrease the initial ion density which in turn results in lower collision frequencies. This process is analogous to decreasing the resistivity of a circuit with a fixed current flowing through it, the result being a drop in the potential.

The kink evident in the lower curve is again a result of the Buneman collision term being triggered as the differential drift velocity exceeds the critical velocity for onset of this phenomenon. From this jump in the potential it is apparent that one could expect turbulence to increase the potential drop across the cloud perhaps by as much as a few volts.

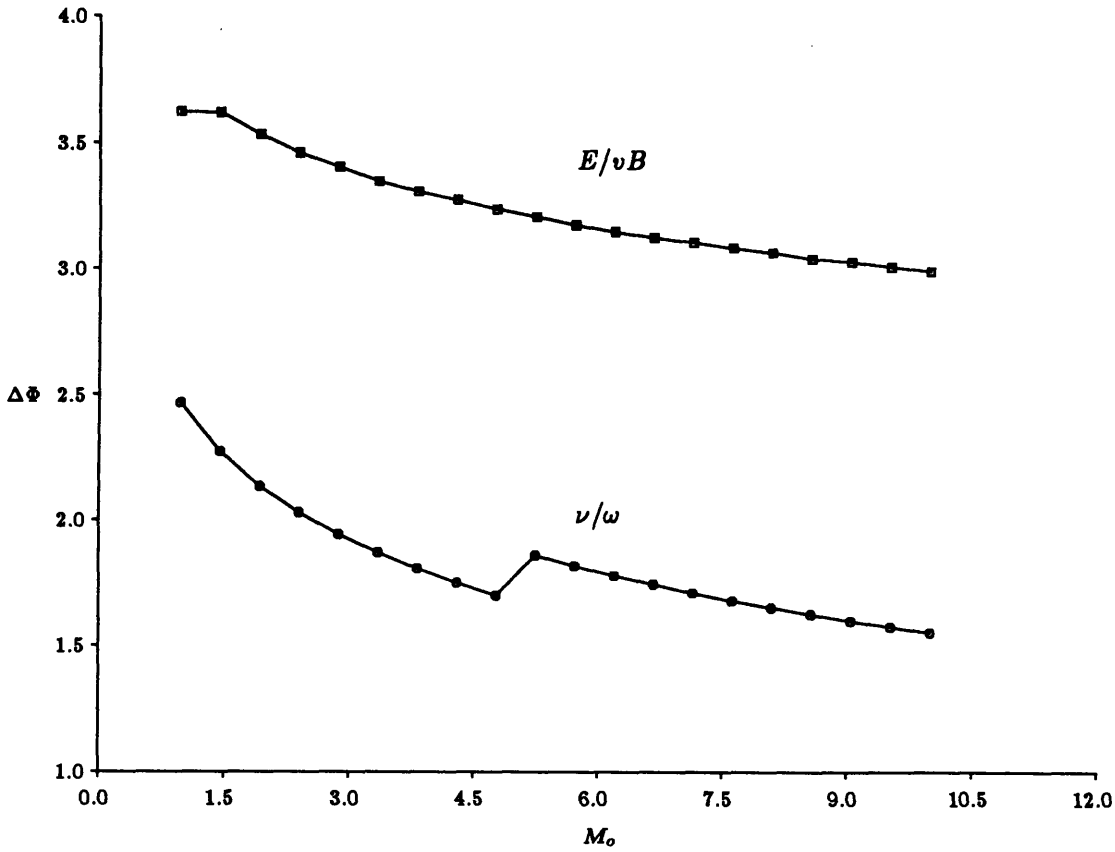

Figure 3.8: Potential Drop vs. Ion Injection Mach No.

3.5 Current Gain

3.5.1 Variation of Current Gain with Ion Current

As mentioned previously, for the currents considered in this study (1.0A and less) ionization was found to play virtually no role in current enhancement. As a consequence the current enhancement can be understood from the standpoint

of random current collection which is the dominant mechanism at work. The electron current collected is given by the random electron flux intersecting the one-dimensional core cloud.

$$I_r = 2\pi r_c^2 e n_{amb}(\sqrt{\frac{eT_e}{2\pi m_e}})$$

where r_c the core radius, n_{amb} is the ambient plasma density and T_e is the electron temperature. The factor of two in the above equation appears as a consequence of the fact that electrons are constrained by the geomagnetic field lines to flow towards the core cloud along a streamtube which intersects the cloud with a total cross-sectional area of $2\pi r_c^2$.

Figure 3.9 shows the gain vs. the logarithm of the contactor ion current. The curve corresponding to the E/vB condition is seen to decrease from a value of 7.95 at 10.0mA to 2.2 at a current of 1.0A. The lower curve corresponding to the collisionality condition is seen to be insensitive with to current with a value of 1.1 over the range considered.

One would expect the gain to increase as a function ion current since the core radius increases and the random current increases as the square of the core radius. This does in fact happen however one must be careful in examining Figure 3.9 to note that the gain I/I_c is defined as the total current divided by the ion current. Since the current with respect to which it is being plotted is increasing exponentially, the denominator will increase faster than the numerator and the gain will decrease with increasing ion current. Conversly, as the current decreases exponentially the gain will increase rapidly.

From the fact the lower curve based on the collisionality condition is relatively constant we can conclude there is virtually no enhancement taking place. For

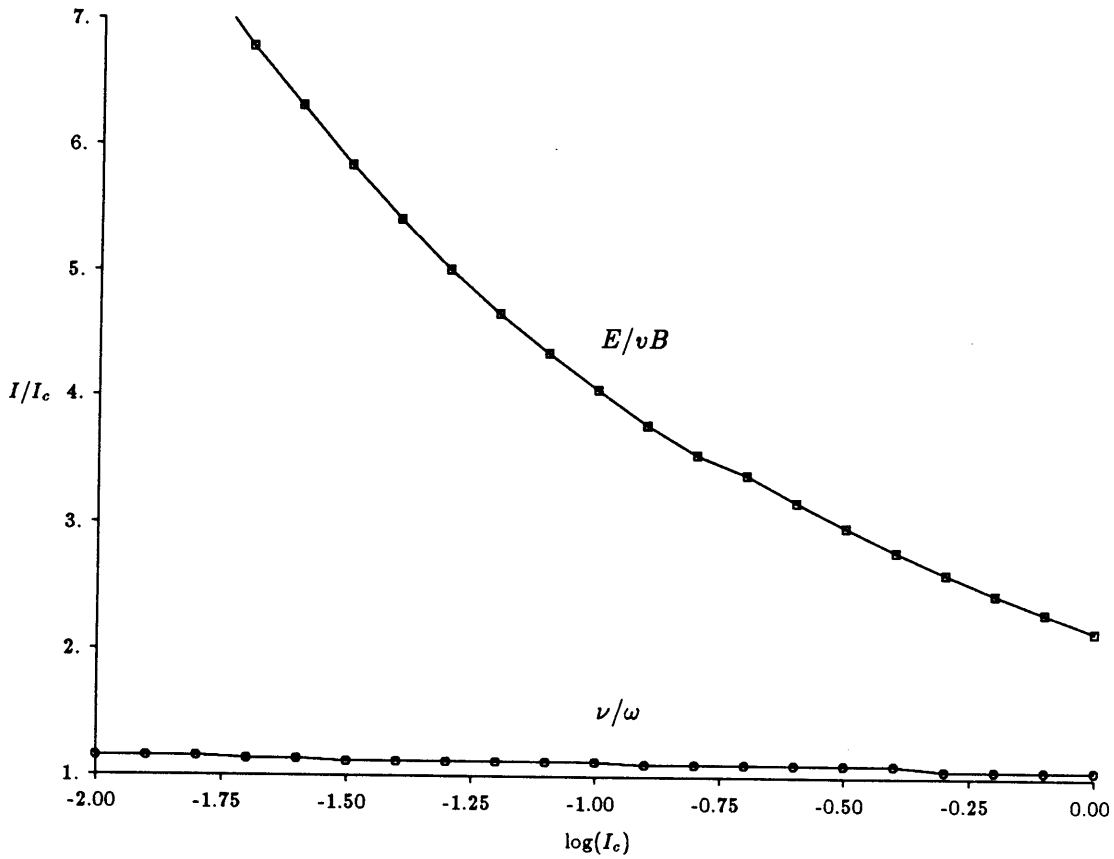

Figure 3.9: Current Gain vs. Log of Ion Current

this curve the total current is approximately the same as the ion current and hence the gain is fixed at a value of roughly one. The reason for this lack of current collection is evident in Figure 3.1 where one can see that the core radius for this curve does not exceed 75 cm. For such a small cloud there is no apparent advantage in using a plasma source.

3.5.2 Variation of Current Gain with Ambient Ion Density

The variation of current gain with ambient ion density is shown in Figure 3.10. The top curve representing the E/vB stopping condition ranges from a value of 1.09 at an ambient density of $10^9 m^{-3}$ up to a value of 2.9 at a density of $10^{13} m^{-3}$. The lower curve representing the collisionality stopping condition ranges from a value of 1.0 at the low end density to a value of 1.3 at the high end.

The curve corresponding to the E/vB stopping condition illustrates the the relative effects of the core radius and ambient density in the equation for the random current. As evident in Figure 3.2 the core radius varies an order of magnitude over the range of ambient densities spanned. Since the random current varies as the radius squared, this would correspond to a two order of magnitude change in the current if the ambient density were constant. Since the ambient density is not constant but rather increases by four orders of magnitude, there is a net increase in the random current collected. The gain was found to increase by a roughly a factor of three. As discussed previously, the actual values obtained for the electron current and core radius are a result of two factors; the

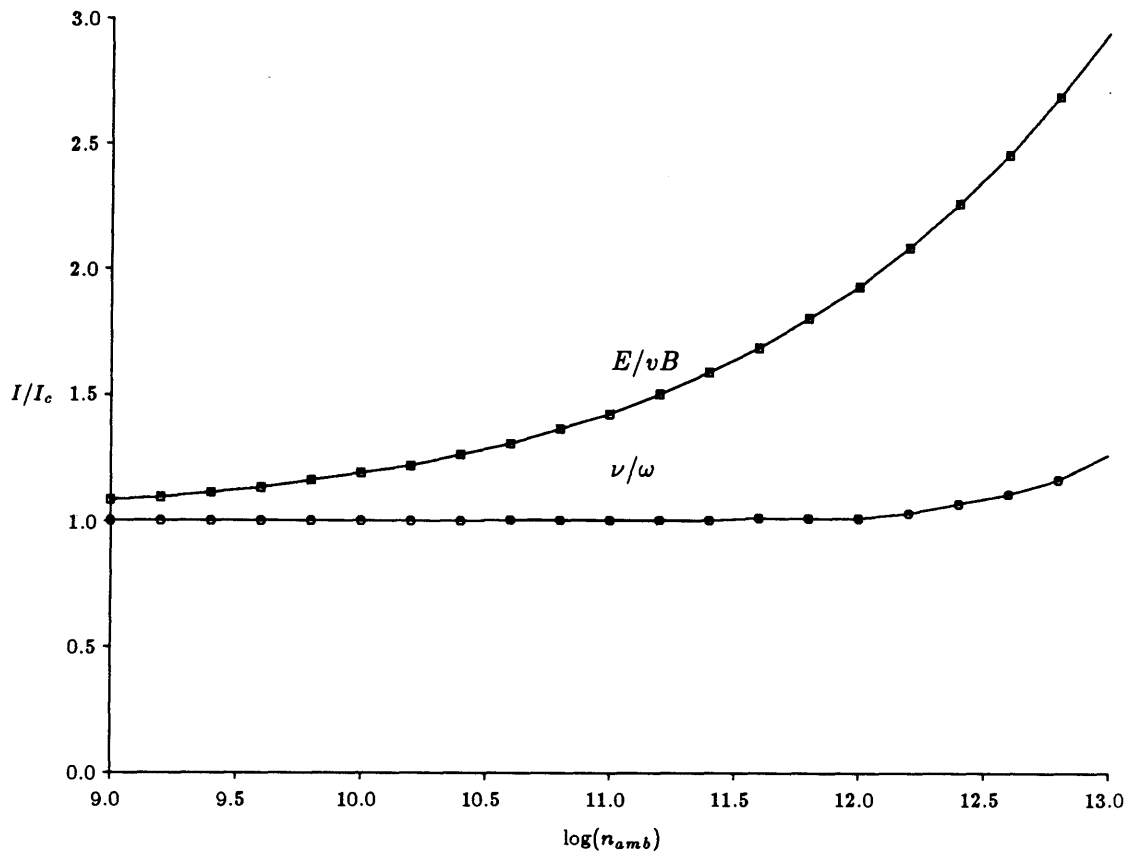

Figure 3.10: Current Gain vs. Log of Ambient Ion Density

core radius decreases with increasing ion current, and the relation of core radius to electron current is specified by the requirement the solution be self-consistent.

In the lower curve of Figure 3.10 corresponding to the collisionality condition, we see the effect upon the gain only due to the increase in ambient density. The reason for this is that the core radius (as evident in Figure 3.2) is independent of ambient density.

3.5.3 Variation of Current Gain with Initial Electron Temperature

Figure 3.11 shows the current gain as a function of initial electron temperature. The upper curve corresponding to the E/vB stopping condition ranges from a value of 2.17 at 0.5eV to a value of 2.67 at 6.7eV. The curve corresponding to the collisionality condition ranges from a value of 1.06 at 0.5eV to a value of 1.75 at 10.0eV.

If one compares the gain curves in Figure 3.11 with the core radius curves in Figure 3.3 the similarity in the shapes of the curves is obvious. This similarity is telling in that it indicates that the gain is being driven by the size of the core cloud. While the mean velocity of the electrons is dependent upon the electron temperature, this is a square root dependence and is therefore not a strong as the dependence on core radii. Furthermore, the electron temperature falls as one moves away form the contactor. The result is that whether the initial electron temperature was 1eV or 10eV, by the time the core is reached it will have fallen somewhat weakening its influence even further. For this reason the discussion of the core radius curves bears directly upon the current enhancement curves as

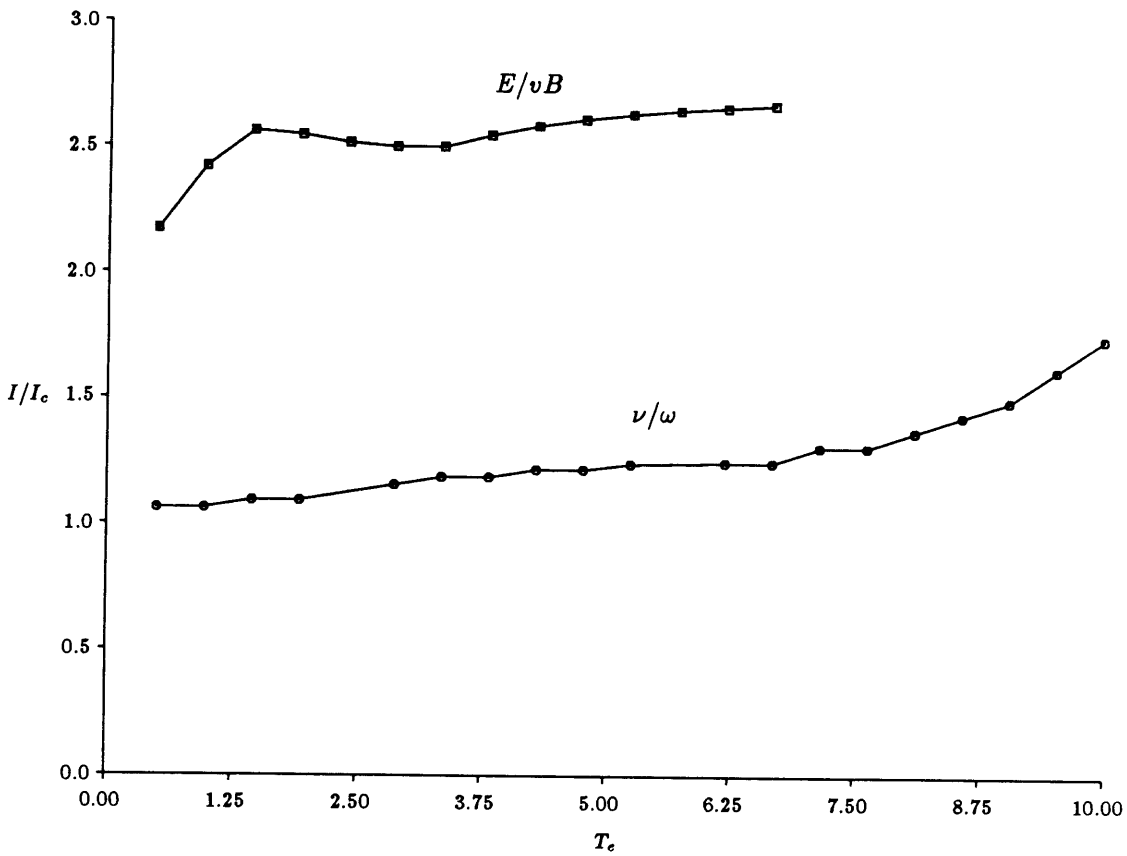

Figure 3.11: Current Gain vs. Initial Electron Temperature

well.

3.5.4 Variation of Current Gain with Injection Mach No.

Figure 3.12 shows the current gain plotted as a function injection mach number. The curve corresponding to the E/vB stopping condition decreases from a value of 2.17 at a mach number of 0.5 to a value of 1.55 for a mach number of 10. The curve corresponding to the collisionality condition is relatively flat with a little variation at each of its extremes. At a mach number of 0.5 the gain is 1.06 and falls to 1.01 at mach 10.

The insensitivity of the curve corresponding to the collisionality condition is easily understood upon inspecting the lower curve in Figure 3.4. The core radius is always less than a meter and changes very little. Thus one does not expect the random current collected to vary.

For the E/vB defined core, the gain curve follows the approximate shape of the core radius curve indicating once again that the collected current is in fact being driven by the size of the core cloud. Since the electron temperature is low (less than 0.5eV) and the ambient ion density is fixed, the current collected must be driven by the core radius.

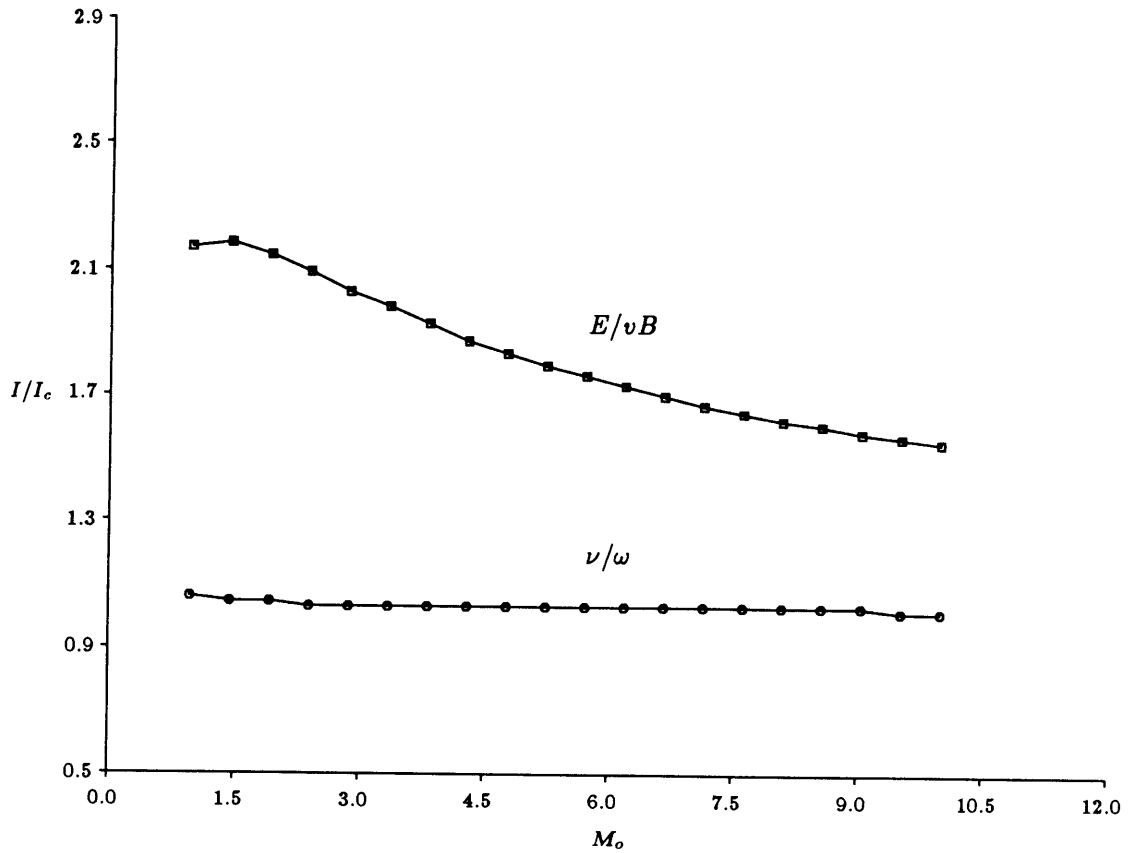

Figure 3.12: Current Gain vs. Ion Injection Mach No.

3.6 Performace Sensitivity to Ionization, Turbulence, and Contactor Radius

A brief effort was undertaken to ascertain the sensitivity of contactor performace to changes in the level of ionization, the presence of turbulence, and the initial radius assumed for the contactor.

3.6.1 Ionization

The cases presented in the preceding figures all assumed an initial degree of ionization of 0.1. The ionization in the emitted plasma is dependent primarily upon the electron temperature and ion current. For this reason, the cases in which the electron temperature was varied from 0.5eV to 10.0eV were expected to best reflect any ionization of neutral which might be occuring.

A set of cases identical to those in Figures 3.3, 3.7, and 3.11 except that ionization was suppressed was run to see the extent of this effect. The results indicated no change in the predicted gains, potential drops, or predicted core radii to within two significant figures.

A closer investigation of one particular case run at 10eV revealed that the ionization rates which are strongly dependent upon the particle densities as well as electron temperature falls off very rapidly since both of these quantities fall off very quickly. Any effect is therefore slight and to a first order both the electron and ion currents are conserverd as well as their sum. Enhancement of current from ionization is not expected to become a significant means of amplification

until one reaches much higher currents, perhaps on the order of hundreds of amperes.

3.6.2 Turbulence

The influence of anomalous resistivity was determined by selectively suppressing these collision terms. While the cases run against ion current, electron temperature, and injection mach number all showed some evidence of turbulent collisions (evident as jumps in the curves), the cases run versus ion current were chosen to study the consequences of suppressing these modes. The reason for this was simply that variation of contactor current seems to be a situation more likely to be seen in reality than changing either the injection mach number or the electron temperature in the region of the contactor.

For the gains, the effect of disabling the turbulence was found to have negligible effect for either of the stopping conditions. Even for the collisionality stopping condition which is directly related to the collision frequencies, the contribution from the anomalous terms was small and did not result in larger cores. For this reason electron current collected from the far field did not change and neither did the gain.

In the case of the potential drops, the E/vB defined core did not change. This was not surprising since the electric field is not as strong a function of collision frequency as the collisionality condition. The potential drop across the core defined by the collisionality condition varied from 0.17V at 10mA to 2.45V at 1.0A. This is compared with 0.35V to 2.45V for the case run with turbulence. The jump in Figure 3.5 has dissapeared indicating the Buneman collision term

contributed roughly 0.17V to the potential drop for currents below 0.4A where it triggered.

The core radius curves for both stopping conditions was virtually unaffected; the small jump in the lower curve of Figure 3.1 dissapearing and the endpoints remaining unchanged.

3.6.3 Contactor Radius

While hollow cathodes do not emit a spherically symmetrical plasma cloud in reality, the model developed here assumed that beyond a certain radius r_o the expansion could in fact be considered to be radial. The purpose then of running some cases at a different value for this radius was to establish a sense of how sensitive the model results are to this assumed radius. The default value used in these simulations was 10cm. Since this is on the order of actual sizes for these devices a more realistic value of the radius at which expansion becomes radial could only be larger than this. For this reason the two sets of runs were done at $r_o = 1.0$m. One set of runs evaluated the effect of this larger initial radius on cases evaluating sensitivity to electron temperature while another examined the effect on cases evaluating sensitivity to ion current.

Most of the effects of increasing the initial radius by an order of magnitude can be anticipated by realizing that for a fixed current, increasing the radius by an order of magnitude will decrease the current density by two orders of magnitude. In addition since the injection velocity is also fixed, the initial ion density will also decrease by two orders of magnitude.

For cases examining the sensitivity to electron temperature, the lower ion density resulted in fewer runs where the integration was able to reach the stopping condition before the density reached the ambient. This was most noticeable in the E/vB stopping condition which has a larger core.

3.6.4 Effect of Larger Initial Radius on Core Radius

Figure 3.13 shows the core radius as a function of electron temperature for the case of $r_o = 1.0m$. This figure is to be compared with Figure 3.3 to see the effects of increasing the initial radius. The core radius is seen to increase from 4.13m at 0.5eV to 5.38m at 2.9eV for the E/vB defined core. The lower curve corresponding to the collisionality stopping condition varies from 1.1m at 0.5eV to 3.73m at 8.1eV.

The primary reason for the larger core radii is the fact the initial radius is larger. While the second term in the simplified electron momentum equation is inversly proportional to the electron density, which will decrease, the density gradient is also affected by the drop in initial ion density. This is clearer in equation (2.15) for the ion density gradient. In addition, the frictional terms which depend upon the density will decrease, further decreasing the initial electric field. For this explanation to be consistent, one should see a decrease in the potential drops even though the core radii is larger.

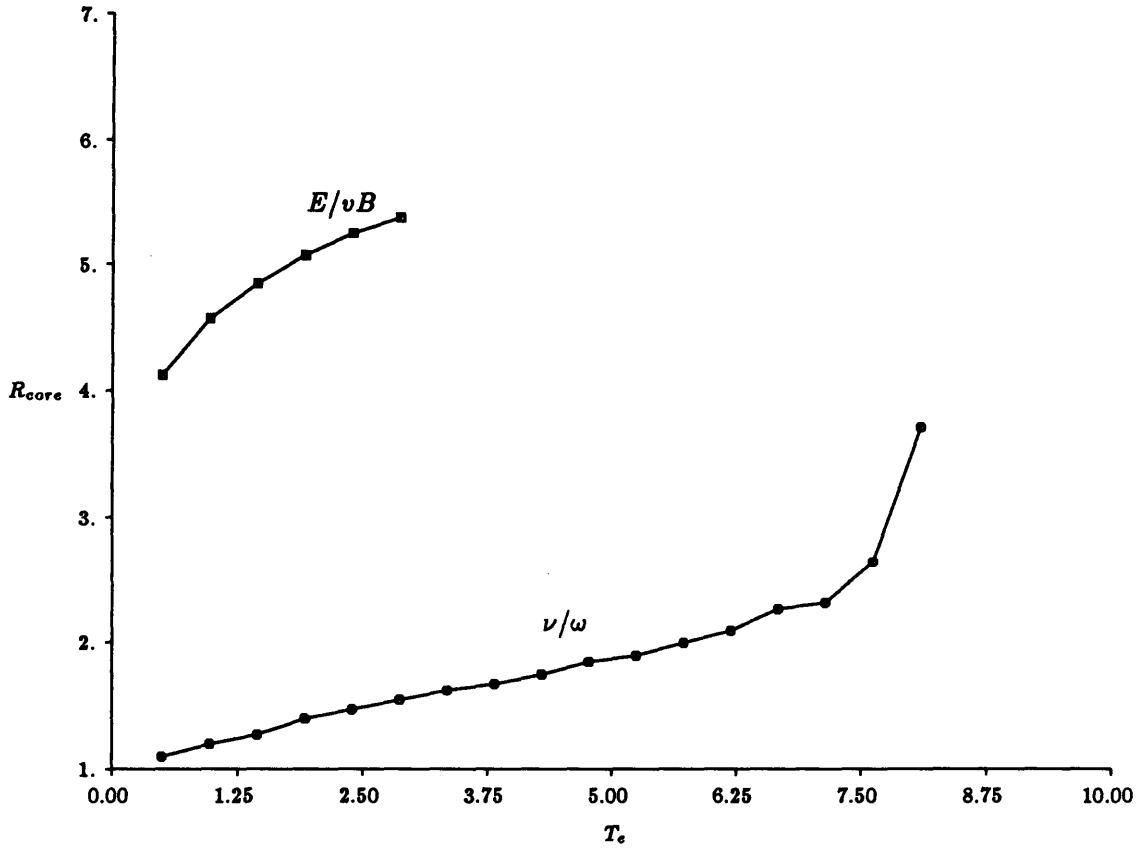

Figure 3.13: Core Radius vs. Initial Electron Temperature: $r_o = 1.0m$

3.6.5 Effect of Larger Initial Radius on Potential Drop

Figure 3.14 shows the potential drop as a function of initial electron temperature for the case of a larger initial radius. Comparing this to Figure 3.7 it is seen that the linearity of the curve defined by the collisionality condition has dissapeared. The potential drop varies from 0.17V at 0.5eV to 23.45V at 8.1eV for this curve. The upper curve representing the E/vB condition is still linear with voltage drops ranging from 1.7V at the lower temperature to 10.74V at 2.9eV.

One might expect that the larger core radii would have resulted in larger potential drops. The potential drops in Figure 3.14 are actually lower than those obtained for the smaller initial radius. While the core radii are in fact larger, the primary reason for this is simply that the integration started at a larger initial radius. The electric field is lower and results in a smaller potential drop.

3.6.6 Effect of Larger Initial Radius on Current Gain

The influence of the larger initial radius on current gain is seen in Figure 3.13. Comparing these results to Figure 3.11 it is evident that the gain has increased somewhat for both boundary conditions. For the E/vB curve, the gain ranges from 2.82 at 0.5eV to 4.10 at 2.9eV. There is less improvement evident in the collisionality curve which ranges from 1.13 at 0.5eV to 2.5 at 8.1eV.

The small increase in the gain is due to the increase in the cloud radius which was observed in Figure 3.13. As was pointed out earlier, the larger core is

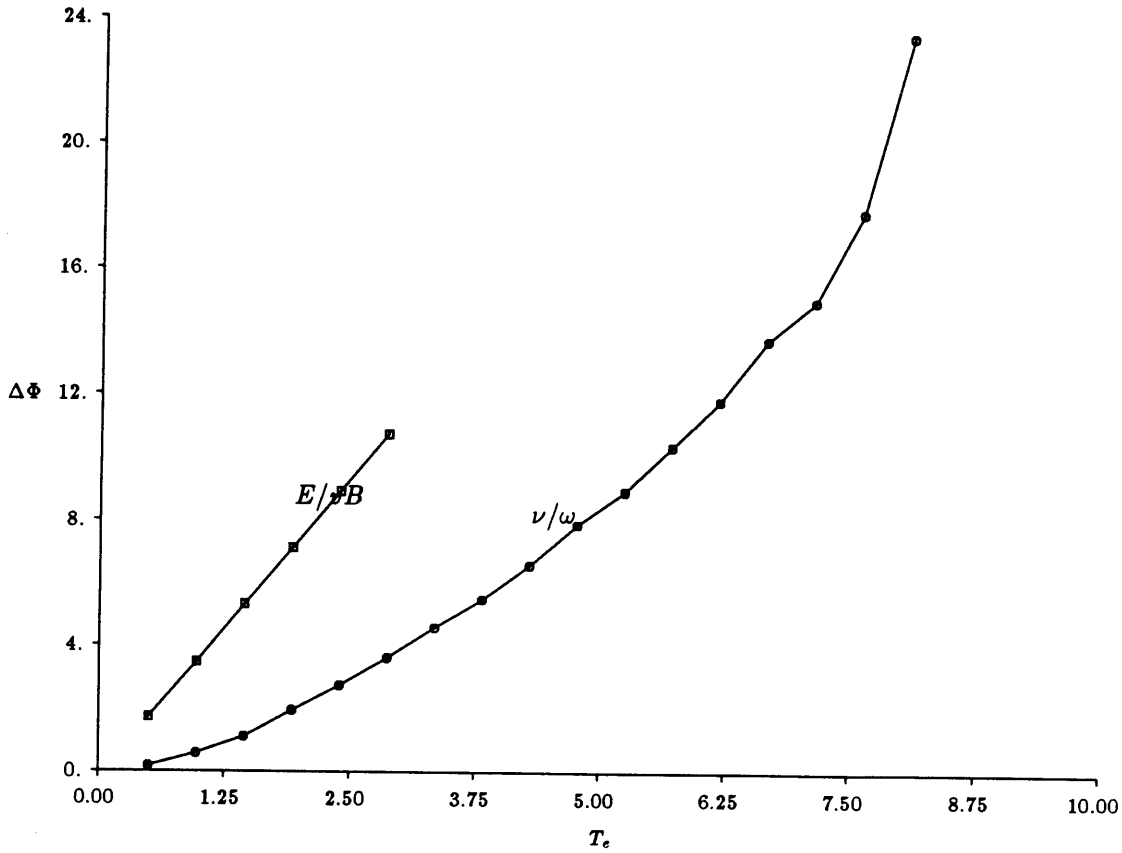

Figure 3.14: Potential Drop vs. Initial Electron Temperature: $r_o = 1.0m$

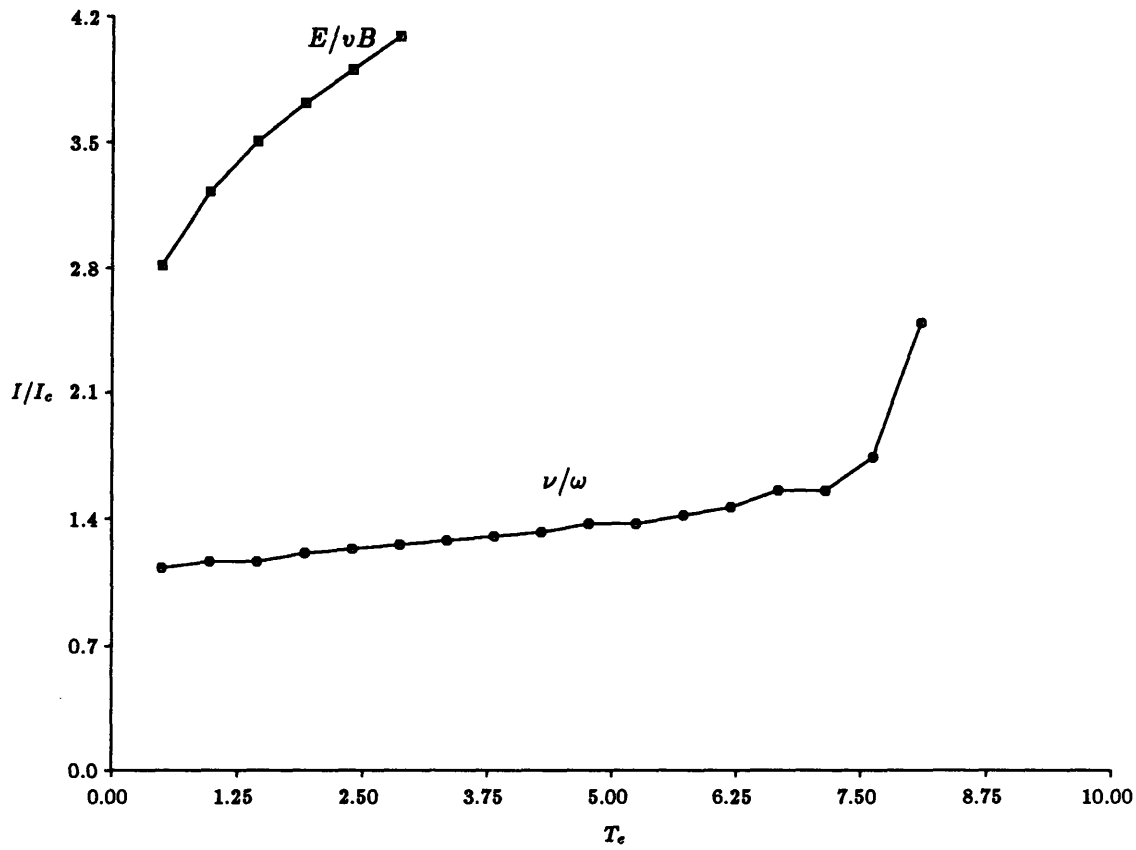

Figure 3.15: Current Gain vs. Initial Electron Temperature: $r_o = 1.0m$

a result of the larger initial radius. Comparing figures 3.13 and 3.15 it is again evident that the core radius drives the gain. The similar shapes of the curves makes this evident.

Chapter 4
Summary and Conclusions

This work has presented the results obtained using a one-dimensional, quasineutral model for the plasma flow associated with the use of plasma contactors. These devices offer a great deal of potential for use in effecting electrical "contact" with the earth's ionosphere. Such contact would be required to complete an electrical circuit consisting of an electrical load associated with a space system, an electrodynamic tether, and the ionospheric plasma environment. Such a tether power system is currently under study and development as a viable alternative to conventional space power systems such as solar arrays and fuel cells.

The numerical model developed as part of this investigation was used to perform a parametric study of plasma contactor performance under a variety of operating conditions. As discussed in the literature and briefly outlined in this thesis, the flow field associated with one of these devices will be multidimensional. The expanding cloud will initially be radial and spherically symmetric to a first order. This dense, one-dimensional, highly collisional core cloud was the focus of the present work. To characterize the performance of a plasma contactor two figures of merit were considered: the current gain or enhancement, and the potential drop associated with the core cloud. In addition, the radius of this core cloud was determined. Sensitivity of these characteristics

to four parameters were investigated in detail; the contactor ion current, the ambient density, the electron temperature in the vicinity of the contactor, and the ion injection mach number. To a lesser extent, the sensitivity to initial ionization fraction, presence of anomalous resistivity, and initial cloud radius was investigated as well.

The core region of the expanding cloud is generally defined as the region within both ion and electrons are unmagnetized. Two criteria were used to determine the bounds on this core. One condition was based on the macroscopic requirement that the radial drift due to the applied electric field dominated the induced $\vec{v_e} \times \vec{B}$ drift. The core boundary using this criteria is defined by the requirement that $E/vB = 1$. The second criteria is a microscopic condition which reflects the fact the electrons are sufficiently collisional so as to prevent them from becoming entrained by the magnetic field lines. This condition is determined from the ratio of electron collision frequency to gyrofrequency. The core boundary using this criteria is defined by the requirement that $\nu/\omega = 1$. The collisionalty or ν/ω condition provides a lower bound on the core radius whereas the E/vB condition provides an upper bound.

Some of the more significant conclusions emerging from this work are now summarized:

The current gain or enhancement was found to increase with decreasing ion current. This implies that these devices could operate more efficiently, in the sense they would carry a larger total current for a given mass flow rate, if operated at lower current levels. It may be advantageous to operate several of these devices in parallel and at lower current than a single device operating at a higher current. As an example, consider a contactor operating at an ion

current of 1A. For the default set of conditions the associated total current will be roughly 2A. For a set of ten contactors operating at 100mA each the total current is closer to 4A for the set of ten. This may introduce other problems if the potential associated with each device is large or if the devices cannot be spaced sufficiently to insure optimal performance. Nevertheless it is an issue which system designers should consider.

Within the limitations of a quasineutral model, the potential drop was found to increase with ion current. This increase was not constant however and appeared to approach some limiting value. Although the size of the core cloud increases with current, most of the potential drop occurs within the first meter of the cloud and as a consequence the potential drop increases at a lower rate than the cloud radius.

The core cloud radius increases with ion current for both of the core defining criteria considered. This would indicate that one could collect more electrons from the far field (since the effective collection area is larger) by operating at higher currents. While this is true, the electron current collected does not increase as fast as the ion current and hence the ratio of collected to emitted current decreases with increasing current.

Because of the consistency condition imposed, the contactor cloud is self adjusting. The consistency condition requires that the electron current collected not exceed the random electron current incident upon the spherical core cloud. As the ambient ion density falls, the consistency condition as well as quasineutrality require the cloud to expand sufficiently to satisfy these two constraints. The consequence of this is that gain varies roughly only by a factor of three while the ambient density may vary four orders of magnitude. This implies op-

eration of these devices may be possible even during the night portion of the spacecraft's orbit.

For the currents and electron temperatures considered, 10mA-1A, and 0.5eV-10eV respectively, ionization was not found to play a significant role in the current enhancement process. Furthermore, the current gain was not found to vary significantly with initial electron temperature.

Potential drops did vary significantly with initial electron temperature indicating that if possible one would want to have cold electrons (on the order of 1eV) in the vicinity of the contactor since this enables the core cloud to expand without incurring to great a penalty in terms of potential drop across the cloud. It is not clear how one could actually control this nor whether the same observation would apply in the presence of double layers.

The current gain varied slightly with variation in ion injection velocity. Generally the gain fell with increasing injection velocity and was maximum for injection velocities just below the ion acoustic speed.

More work needs to be done in order to better understand the significance of contactor plasma behavior in terrestrial laboratories, especially with respect to the formation of double layers.

Appendix A
Contactor Program Listing

The main calling program called ITETHER controls data input, iteration to find self-consistent potential, and evaluation of stopping conditions.

A.1 Main Program

```
      PROGRAM ITETHER
C
C     THIS PROGRAM CALCULATES THE QUASINEUTRAL POTENTIAL AND
C     ION DENSITY PROFILES FOR A PLASMA CONTACTOR
C
      IMPLICIT REAL*8(A-H,O-Z)
      REAL*8 MP,MIC,ME,KAPPA,LAMBDAC,LAMBDAO,MASSIC,MIO,MASSIO,
     $           MACHION,JIC,JIO,JE
      INTEGER*4 STPSTOP,TRYSTOP,PRNTCOM
      DIMENSION F(9),DF(9),RWORK(184),IWORK(29),CELE(100),CMAX(100)
     $          ,CTOT(100),XNUE(6),ATOL(9)
      NAMELIST/INPUTDAT/CURICO,CUREO,POTO,EO,TEO,DENEO,QDOTO,VICOO,
     $         RO,RFIN,TEAMB,DENIAMB,MASSIO,EIONO,TIOO,SIGENO,FRACIO,ZO,
     $         MASSIC,EIONC,TICO,SIGENC,FRACIC,ZC,STEPFAC,IPLOT,STPSTOP,
     $         IQUAS,IDIREC,INTER,MACHION,DENFAC,ITURB,HIFAC,IONREC,
     $         ISTOP
C
```

```
      DATA PERMIT,B,EC,ME,MP/8.8542E-12,0.45E-4,1.6022E-19,
     $     9.1095E-31,1.67265E-27/
      EQUIVALENCE(DENNC,F(1)),(DENIC,F(2)),(POT,F(3)),(QDOT,F(4)),
     $          (TE,F(5)),(DENE,F(6)),(E,F(7)),(DENIO,F(8)),
     $          (DENNO,F(9))
      COMMON/PARAM/CS,RO,DENICO,POTO,QDOTO,EO,TEO,SO,
     $ EISTAR,EESTAR,PSTAR,TESTAR,XNUE,EVB,CURICO,COLL,
     $ TIC,TIO,EIONC,EIONO,MIC,MIO,ZC,ZO,SIGENC,SIGENO,MASSIC,MASSIO,
     $ VE,VIC,VICO,POTO,DENIAMB,PI,KAPPA,CURT,CURE,CURIC,CURRAN,DEDRO,
     $ DENNC,DENIC,POT,QDOT,TE,DENE,E,DENIO,DENNO,BETA
C
      COMMON/FLAG/ISTEP,IQUAS,IDIREC,ITURB
      COMMON/GRAD/IONREC,JIC,JE,JIO,VEO,TEAMB
      EXTERNAL GRAD,JAC
C
      OPEN(UNIT=50,FILE='IDATA.IN',STATUS='OLD')
      OPEN(UNIT=7,FILE='CURENT.DAT',STATUS='NEW')
C
C
C***********************************************************************
C     The various control switches used to alter the solution model
C     and presentation are defined below:
C
C     IPLOT   This turns the plotting subroutine on (IPLOT=1) or
C             off(IPLOT=0). It will plot either the full number of
C             steps in the solution or up until the value of STPSTOP
C             (whichever comes first)
C
C     IQUAS   This selects the set of governing equations used in the
C             solution. The most general set is obtained using (IQUAS=0).
C             The quasi-neutral set is invoked when (IQUAS=1)
C
```

```
C     IDIREC  This controls the direction of the integration. (IDIREC=1)
C             results in an inward integration (RO > RFIN). (IDIREC=0)
C             is used for an outward integration (RFIN < RO).
C
C     INTER   This turns the iterator which insures the consistency of
C             the final current solution on (INTER=1) or off (INTER=0)
C             INTER=1 is only used for outward solutions ie. IDIREC=0
C             The first guess on electron current (CUREO)is determined
C             by the selected value of HIFAC. (ie. CUREO=HIFAC*CURICO).
C
C     ITURB   This turns on the ion acoustic and Bunemann collision
C             terms for (ITURB=1) or off (ITURB=0).
C
C     IONREC  This turns on the ionization and recombination collisions
C             for (IONREC=1) or off for(IONREC=0)
C
C     ISTOP   This determines the criteria used to define the core
C             cloud. The E/vB condition is invoked when ISTOP=1
C             where as the collisionality condition is used when
C             ISTOP=0.
C
C
C*************************************************************************
C
      READ(50,INPUTDAT)
C
      PI=DACOS(-1.DO)
      MIC=MASSIC*MP
      MIO=MASSIO*MP
C
C*************************************************************************
C
```

```
C     ISTEP is the count of actual steps taken in the integration
C           thus far. The initial conditions correspond to ISTEP=1
C           so ISTEP=2 indicates the first step taken by LSODE.
C
C     LOOP1 is the counter of iterations used when INTER=1 and the program
C           is solving for a consistent current solution.
C
C*************************************************************************
C
      LOOP1=0
C
C
C*************************************************************************
C
C     The consistent solution of the electron current uses a bisection
C     algorithm with the initial low guess for CUREO of 0 and a high
C     guess determined by HIFAC. At any point, the high and low guesses are
C     bracketed by CHI and CLO respectively.
C
C*************************************************************************
C
      IF(INTER.EQ.1)THEN
         CLO=0.0
         CHI=HIFAC*CURICO
         CUREO=(CHI+CLO)/2.0
      ENDIF
C
20    CONTINUE
      LOOP1=LOOP1+1
      CURIC=CURICO
      CURE=CUREO
      POT=POTO
```

```
      E=EO
      TE=TEO
      DENE=DENEO
      QDOT=QDOTO
      VIC=VICOO
      R=RO
C
      CURICO=CURIC
      CS=DSQRT(2.0*TE*EC/MIC)
C
C*************************************************************************
C
C     When INTER=0, any initial value can be selected for the ion drift
C     velocity VICOO. When INTER=1 the initial ion velocity is expressed
C     as some multiple of the ion acoustic speed (not necessarily 1.0).
C     This value is inputed as MACHION.
C
C*************************************************************************
C
      IF (INTER.EQ.1)VIC=MACHION*CS
C
C
C*************************************************************************
C
C     The following IF block determines the initial ion and electron
C     densities. All densities are normalized with respect to the ambient
C     ion density DENIAMB.
C
C     For an inward solution (IDIREC=1) The ion density is set to ambient
C     since quasi-neutrality is assumed. Neutral densities are determined
C     from the assumed value of ionization fraction. Electron density is
C     the sum of ambient ion density and contactor ion density multiplied
```

```
C     by a factor (DENFAC) which is normally equal to one.
C
C     For an outward solution (IDIREC=0) The ion density is determined
C     from the definition of ion current and electron density is determined
C     in the same manner as for the inward solution.
C
C
C*************************************************************************
C
      DENICO=DENIAMB
C
      IF(IDIREC.EQ.1)THEN
C
      DENIO=1.0
      DENNO=(1.0-FRACIO)/FRACIO
      DENIC=1.0
      DENNC=(1.0-FRACIC)/FRACIC
      DENE=DENFAC*DENIC+DENIO
      ELSE
      DENIO=1.0
      DENIC=CURIC/(VIC*EC*4.0*PI*R**2)/DENICO
      DENNO=DENIO*(1.0-FRACIO)/FRACIO
      DENNC=DENIC*(1.0-FRACIC)/FRACIC
      DENE=DENFAC*DENIC+DENIO
C
      ENDIF
C
C
C
C*************************************************************************
C
C     The following block calculates the characteristic values used
```

```
C     in the normalization.
C
C*************************************************************************
C
      RO=DSQRT(PERMIT*TE/((1.0+DENFAC)*DENIAMB*EC))
      RSTEP=STEPFAC*(RO/RO)
      POTO=TEAMB
      TEO=TEAMB
      EO=POTO/RO
      SO=CS*DENICO/RO
      QDOTO=(CURICO/(4.0*PI*R**2.0))*TE
      VDSTAR=CURICO/((4.0*PI*RO**2)*EC*DENICO)
      DEDRO=(PERMIT*EO)/(EC*DENICO*RO)
C
C
C*************************************************************************
C
C      Following parameters are groupings of variables which appear
C      frequently in the governing equations.
C
C*************************************************************************
C
      PSTAR=EC*POTO
      EISTAR=MIC*CS**2
      EESTAR=ME*CS**2
      TESTAR=EC*TEO
C
C
C
C
C*************************************************************************
C
```

```
C     IFLAG2  This is set to a value of 1 when ISTEP has reached
C             STPSTOP or the integration has been completed. This in
C             effect then notifies the plotting subroutine that
C             the variables currently stored will be the set plotted.
C
C     IFLAG3  Inspection of results using the plotter is done interactively
C             using a menu. When the menu is exited, IFLAG3 is set to 1
C             and control is returned to the main program.
C
C*************************************************************************
C
      IFLAG2=0
      IFLAG3=0
C
      ISTEP=1
C
C
C*************************************************************************
C
C     In the following block, initial values which have been inputted
C     in real units are normalized. All calculations of gradients etc.
C     are performed with equations in non-dimensional form.
C
C*************************************************************************
C
      R=R/RO
      RFIN=RFIN/RO
      RSTART=R
      POT=POT/POTO
      TE=TE/TEO
      E=E/EO
      CURIC=CURIC/CURICO
```

```
      POTO=POT
C
C
C
C***********************************************************************
C
C     For inward solution (IDIREC=1), the initial ion velocity is
C     is calculated from the ion current and density. Since solution
C     begins in the far field, the electron current is determined from
C     the random electron thermal flux. The sum of the ion and electron
C     currents define the maximum current (CURMAX) which for this mode
C     of solution is equal to the total current (CURT) by definition.
C     Therefore to obtain a consistent solution in this mode requires
C     the initial ion current to be varied.
C
C     For an outward solution (IDIREC=0), there are two possibilities:
C      If the iteration solver has been engaged (INTER=1) then the initial
C      ion velocity is just some multiple of the ion accoustic velocity
C      (MACHION). Also, the initial heat flux is taken to be the electron
C      thermal flux which is also the characteristic value used for
C      normalization.(ie. QDOT is set to 1.0)
C
C      If the iteration solver has been disengaged (INTER=0), then the
C      initial inputed value for the ion velocity (in real units) is
C      normalized with respect to the ion acoustic velocity. Similarly,
C      the initial heat flux is normaslized with respect to the electron
C      thermal flux.
C
C     The electron current is the initial value normalized with respect
C     to the ion current, and the total current is the sum of the ion and
C     electron currents. In this mode, a consistent solution is achieved
C     when the maximum current, which is the sum of the ion and random
```

```
C     thermal electron current is equal to the total current. Therefore
C     to acheive a consistent solution in this mode the initial electron
C     current must be varied.
C***********************************************************************
C
C
      IF(IDIREC.EQ.1)THEN
C
         VICO=CURIC/(DENIC*R**2)*(VDSTAR/CS)
         CURE=(R**2)*(DENIAMB/DENICO)*DSQRT(TEAMB/TEO)*(DSQRT(TESTAR/
     $        (2.0*PI*ME))/(2.0*VDSTAR))
         CURMAX=CURIC+CURE
         CURT=CURMAX
      ELSE
C
         IF(INTER.EQ.1)THEN
            VICO=MACHION
            QDOT=1.0
         ELSE
            VICO=VIC/CS
            QDOT=QDOT/QDOTO
         ENDIF
C
         CURE=CURE/CURICO
         CURT=CURIC+CURE
      ENDIF
C
      TIC=TICO/TEO
      TIO=TIOO/TEO
C
C
      VEO=(CURE/(DENE*R**2))*(VDSTAR/CS)
```

```
C
C
C
C***********************************************************************
C
C     The following block set up the parameters to initialize the
C     LSODE solver. The various meanings of these parameters can
C     be found in the comments for the original LSODE source code.
C
C***********************************************************************
C
      NEQ=9
      R1=R
      R2=R
      ITOL=2
      RTOL=1.0D-4
      ATOL(1)=1.0D-1
      ATOL(2)=1.0D-4
      ATOL(3)=1.0D-4
      ATOL(4)=1.0D-4
      ATOL(5)=1.0D-3
      ATOL(6)=1.0D-4
      ATOL(7)=1.0D-6
      ATOL(8)=1.0D-10
      ATOL(9)=1.0D-6
      ITASK=1
      ISTATE=1
      IOPT=1
      LRW=22+9*NEQ+NEQ**2
      DO 30 J=1,LRW
        RWORK(J)=0.0
30    CONTINUE
```

```
      LIW=20+NEQ
      DO 35 J=1,LIW
        IWORK(J)=0
        IF(J .EQ. 6)IWORK(6)=1000
35    CONTINUE
      MF=22
      ICORE=0
C
C
C
C***********************************************************************
C
C     First call to GRAD evaluates derivatives at initial point.
C     If the quasi-neutral set of equations is being used, (IQUAS=1)
C     then the electric field is calculated from the potential gradient.
C     Otherwise, it is determined form the Poisson equation.
C
C
C***********************************************************************
C
      IF(IQUAS.EQ.1)THEN
       VE=(CURE/(DENE*R**2))*(VDSTAR/CS)
      ELSE
       VE=DSQRT(2*PSTAR/EESTAR*(POT-POTO)+VEO**2)
      ENDIF
C
      CALL GRAD(NEQ,R,F,DF)
      IF(IQUAS.EQ.1) E=-DF(3)
C
50    IF(IDIREC.EQ.1)THEN
        R2=R1-RSTEP
      ELSE
```

```
        R2=R1+RSTEP
      ENDIF
C
C
       IF(IPLOT .EQ. 1)THEN
       IF(ISTEP.EQ. STPSTOP)IFLAG2=1
         CALL PLOT(R,F,DF,ISTEP,IFLAG2,IFLAG3,STPSTOP)
       ENDIF
      ISTEP=ISTEP+1
C
      IF(IFLAG3.EQ.1)GO TO 1000
C
      CALL LSODE(GRAD,NEQ,F,R1,R2,ITOL,RTOL,ATOL,ITASK,ISTATE
     $           ,IOPT,RWORK,LRW,IWORK,LIW,JAC,MF)
C
C
      R=R1
C
      IF(IQUAS.EQ.1) E=-DF(3)
C
C
C
C***********************************************************************
C
C     ISTATE is the LSODE error flag. The meaning of various negative
C     values of ISTATE can be found in the  source code for LSODE.
C
C***********************************************************************
C
      IF(ISTATE .LE. 0) GO TO 1000
C
C
```

```
      IF(IQUAS.EQ.1)THEN
       VE=(CURE/(DENE*R**2))*(VDSTAR/CS)
      ELSE
       VE=DSQRT(2*PSTAR/EESTAR*(POT-POTO)+VEO**2)
      ENDIF
C
      CALL GRAD(NEQ,R,F,DF)
      IF(IQUAS.EQ.1) E=-DF(3)
C
C
C*************************************************************************
C
C      Ion and electron velocities and currents are calculated based
C      on the latest values to have been computed by LSODE. Under some
C      circumstances, (ie. high ionization and low initial electron current
C      guess) the ion current will exceed the total current and the
C      electron velocity becomes negative. This condition will terminate
C      the current iteration step, a new electron current will be
C      calculated and solution attempted again.
C
C*************************************************************************
C
      VIC=DSQRT(VICO**2-2.0*PSTAR/EISTAR*(POT-POTO))
      CURIC=VIC*DENIC*R**2*(CS/VDSTAR)
      CURE=CURT-CURIC
      IF(IQUAS.EQ.1)THEN
       VE=(CURE/(DENE*R**2))*(VDSTAR/CS)
      ELSE
       VE=DSQRT(2*PSTAR/EESTAR*(POT-POTO)+VEO**2)
      ENDIF
C
      IF(VE.LE.0.0)GO TO 55
```

```
C
C
C*************************************************************************
C
C     The ratio E/vB is calculated. If the iterative solver has been turned
C     off, (INTER=0) then marching is stoppep by setting STPSTOP equal to
C     the current ISTEP when the stopping criteria is satisfied. The value
C     of the collisionality COLL is calculated is GRAD and so its most
C     current value is already available from the last call to GRAD.
C
C*************************************************************************
C
      BETA=DENE*EC*DENICO*(TE+TIC)*TEO*2.52E-6/(B**2)
      IF(BETA .GE. 1.0)THEN
        EVB=100.0
        ELSE
        BMOD=DSQRT(1-BETA)*B
        EVB=DABS(E/(VE*BMOD))*EO/CS
      ENDIF
      IF(BETA.GT. 1.0) RBETA=R*RO
C
C      IF(INTER .NE. 1)THEN
C        IF(((EVB.LE.1.0).AND.(ISTOP.EQ.1)).OR.((COLL .LE.1)
C     $        .AND.(ISTOP.EQ.0)))THEN
C          STPSTOP=ISTEP
C          GO TO 1000
C        ENDIF
C      ENDIF
C
      RDIFF1=RSTART-R
      RDIFF2=RSTART-RFIN
      RFRAC=RDIFF1/RDIFF2
```

```
C
C
C*****************************************************************************
C
C     If the marching direction is outward, (IDIREC=0) then the random
C     electron thermal current is evaluated in the far field based on
C     the ambient electron temperature and density.
C
C*****************************************************************************
C
      IF(IDIREC.EQ.0) THEN
        CURRAN=(R**2)*(DENIAMB/DENICO)*DSQRT(TEAMB/TEO)*
     $(DSQRT(TESTAR/(2.0*PI*ME))/(2.0*VDSTAR))
        CURMAX=CURIC+CURRAN
      ENDIF
C
C
C*****************************************************************************
C
C     The following block determines whether the integration has
C     been completed depending on the  mode of operation being used.
C     If the solution is based on an inward marching direction (IDIREC=1)
C     then integration is stopped if R=RFIN  (RSTART>RFIN) otherwise
C     control is returned to LSODE for another step. If the marching
C     direction is outward (IDIREC=0), then:
C        If the iterative solver has been engaged, (INTER=1) integration
C        is stopped when the appropriate stopping criteria has been met.
C        If the iterative solver has been deisengaged (INTER=0) then
C        integration is stopped when R=RFIN (RSART<RFIN)
C
C*****************************************************************************
C
```

```
      IF(IDIREC.EQ.1)THEN
        IF(R .GT. RFIN) GO TO 50
      ELSE
        IF(INTER.EQ.1)THEN
           IF(ISTOP.EQ.1)THEN
              IF(EVB .GE. 1.00) GO TO 50
           ELSE
             IF(COLL .GE. 1.00) GO TO 50
           ENDIF
        ELSE
           IF(R .LT. RFIN)GO TO 50
        ENDIF
      ENDIF
C
C
C*************************************************************************
C
C     If the iterative solver has been engaged,(INTER=1) then the following
C     block compares the total and maximum currents to evaluate the level
C     of convergence. Both the difference and fractional error are
C     calculated. If the solution has not yet converged, then a new
C     initial electron current guess is made (CUREO) and control is
C     is returned to the begining of the program.
C
C*************************************************************************
C
55    IF((IDIREC.EQ.0).AND.(INTER.EQ.1))THEN
        DIFF1=(CURMAX-CURT)
        ERROR1=DIFF1/CURMAX
        WRITE(6,56)LOOP1,DIFF1,ERROR1,ISTEP
56      FORMAT(1X,'LOOP1=',I4,2X,'DIFF1=',1PE10.3,2X,'ERROR1=',
     $  1PE10.3,2X,'ISTEP=',I4)
```

```
        CELE(LOOP1)=CUREO/CURICO
        CMAX(LOOP1)=CURMAX
        CTOT(LOOP1)=CURT
        IF(LOOP1.GT.25) GO TO 1000
        IF((DABS(DIFF1).GT.0.01).AND.(DABS(ERROR1).GT.0.01))THEN
          IF(DIFF1.GT.0.0)THEN
            CLO=CUREO
          ELSE
            CHI=CUREO
          ENDIF
          CUREO=(CLO+CHI)/2.0
          GO TO 20
        ENDIF
      ENDIF
C
1000  CONTINUE
C
      DO 200 I=1,LOOP1
      WRITE(7,57) CELE(I),CMAX(I)
57    FORMAT(1X,1PE11.4,2X,1PE11.4,2X)
200   CONTINUE
C
C
      DO 201 I=1,LOOP1
      WRITE(7,58) CELE(I),CTOT(I)
58    FORMAT(1X,1PE11.4,2X,1PE11.4,2X)
201   CONTINUE
C
       IFLAG2=1
       IF(IPLOT .EQ. 1)THEN
         CALL PLOT(R,F,DF,ISTEP,IFLAG2,IFLAG3,STPSTOP)
       ENDIF
```

```
C
      IF(VE.LE.0.0)THEN
       WRITE(6,68)
68     FORMAT(1X,' EXECUTION ABORTED DUE TO NEGATIVE VALUE OF VE')
      ENDIF
      IF(CUREO.LT.0.0)THEN
       WRITE(6,69)
69     FORMAT(1X,' EXECUTION ABORTED DUE TO NEGATIVE VALUE OF CUREO')
      ENDIF
C
      IF(ISTATE .LE. 0) THEN
       WRITE(6,70)ISTATE
70     FORMAT(' EXECUTION ABORTED DUE TO LSODE ERROR FLAG: ISTATE=',I4)
      ENDIF
C
      IF(DENIC.LE.DENIO) THEN
       WRITE(6,71)
71     FORMAT(' ION DENSITY REACHED AMBIENT ION DENSITY IN THIS RUN ')
      ENDIF
C
      REND=R*RO
      WRITE(6,80)REND,ISTEP,RO,RFRAC
80    FORMAT(1X,'R (m)=',1PE11.4,2X,'ISTEP=',I5,2X,'RO=',1PE11.4,
     $ 2X,'RFRAC=',1PE11.4)
C
      CURIC=CURIC*CURICO
      CURE=CURE*CURICO
      POT=POT*POTO
      E=E*EO
      TE=TE*TEO
      DENE=DENE*DENICO
      QDOT=QDOT*QDOTO
```

```
      VIC=VIC*CS
      GAIN=CUREO/CURICO
C
      WRITE(6,81) CURIC
81    FORMAT('  CURIC=',1PE12.5)
      WRITE(6,86) CURE
86    FORMAT('  CURE=',1PE12.5)
      WRITE(6,82) POT
82    FORMAT('  POTENTIAL=',1PE12.5)
      WRITE(6,83) E
83    FORMAT('  E FIELD=',1PE12.5)
      WRITE(6,84) TE
84    FORMAT('  ELEC TEMP=',1PE12.5)
      WRITE(6,85) DENE
85    FORMAT('  DENE=',1PE12.5)
      WRITE(6,87) QDOT
87    FORMAT('  QDOT=',1PE12.5)
      WRITE(6,88) VIC
88    FORMAT('  VIC=',1PE12.5)
      WRITE(6,89) REND
89    FORMAT('  R=',1PE12.5)
      WRITE(6,90) GAIN
90    FORMAT('  GAIN=',1PE12.5)
      WRITE(6,91) RBETA
91    FORMAT('  RBETA=',1PE12.5)
C
      CALL EXIT
      END
C
C
```

A.2 Plotting Subroutine: PLOT

The subroutine PLOT controls the storage and display of various profiles when the program is being used interactively.

```
      SUBROUTINE PLOT(R,F,DF,ISTEP,IFLAG2,IFLAG3,STPSTOP)
      IMPLICIT REAL*8(A-H,O-Z)
      REAL*8 MP,MIC,ME,KAPPA,LAMBDAC,LAMBDAO,MASSIC,MIO,MASSIO
      REAL*4 X,Y,YPL,DEDR,EGRAD,YSTORE
      INTEGER*4 STPSTOP,PCOM
      DATA PERMIT,B,EC,ME,MP/8.8542E-12,0.45E-4,1.6022E-19,
     $     9.1095E-31,1.67265E-27/
      CHARACTER*80 PLT,TIT,TITLE,PLOTITL
      DIMENSION X(9000),Y(2,9,9000),F(9),DF(9),
     $ YPL(9000),YSTORE(6,9000),PLT(9,2),TIT(9,2),N(2),
     $ IOPT(2),XNUE(6),DEDR(9000)
      COMMON/PARAM/CS,RO,DENICO,POTO,QDOTO,EO,TEO,SO,
     $ EISTAR,EESTAR,PSTAR,TESTAR,XNUE,EVB,CURICO,COLL,
     $ TIC,TIO,EIONC,EIONO,MIC,MIO,ZC,ZO,SIGENC,SIGENO,MASSIC,MASSIO,
     $ VE,VIC,VICO,POTO,DENIAMB,PI,KAPPA,CURT,CURE,CURIC,CURRAN,DEDRO,
     $ DENNC,DENIC,POT,QDOT,TE,DENE,E,DENIO,DENNO,BETA
C
C
      PLT(1,1)='R       n_o     n_o* = Ambient Density  '
      PLT(2,1)='R       n_+     n_+* = Ambient Density  '
      PLT(3,1)='R       POT     '
      PLT(4,1)='R       QDOT    Qdot* = Heat flux at Ro in (W/m2) '
      PLT(5,1)='R       T_e     '
      PLT(6,1)='R       n_e     n_e* = Ambient Density  '
      PLT(7,1)='R       E       '
      PLT(8,1)='R       EvB Coll '
      PLT(9,1)='R       VD/VE   '
```

```
C
      PLT(1,2)='R       nue  '
      PLT(2,2)='R       nue  '
      PLT(3,2)='R       nue      '
      PLT(4,2)='R       dQ/dR    '
      PLT(5,2)='R       dT_e/dR  '
      PLT(6,2)='R       dn_e/dR  '
      PLT(7,2)='R       dE/dR    '
      PLT(8,2)='R       Ve Vi    Normalized with respect to Ion
     $ Acoustic Velocity'
      PLT(9,2)='R       Ie Ii    Normalized with respect to Ion
     $ current'
C
C
      TIT(1,1)='CONTACTOR NEUTRAL DENSITY VS. RADIAL POSITION'
      TIT(2,1)='CCONTACTOR ION DENSITY VS. RADIAL POSITION'
      TIT(3,1)='PPotential vs. Radial Positio '
      TIT(4,1)='HEAT FLUX VS. RADIAL POSITION'
      TIT(5,1)='Electron Temperature vs. Radial Position'
      TIT(6,1)='ELECTRON DENSITY VS. RADIAL POSITION'
      TIT(7,1)='Electric field vs. Radial position'
      TIT(8,1)='EVB & COLL VS RADIAL POSITION'
      TIT(9,1)='RATIO OF DRIFT TO ELECTRON VELOCITY VS RADIAL POSITION'
C
C
      TIT(1,2)='ION ACOUSTIC COLLISION RATE'
      TIT(2,2)='BUNEMANN COLLISION RATE'
      TIT(3,2)='Total Elastic Collision Frequency'
      TIT(4,2)='GRADIENT OF HEAT FLUX VS. RADIAL POSITION'
      TIT(5,2)='GRADIENT OF ELECTRON TEMPERATURE VS. RADIAL POSITION'
      TIT(6,2)='GRADIENT OF ELECTRON DENSITY VS. RADIAL POSITION'
      TIT(7,2)='GRADIENT OF ELECTRIC FIELD VS. RADIAL POSITION'
```

```
      TIT(8,2)='Normalized Ion and Electron Drift Velocity'
      TIT(9,2)='Normalized Ion and Electron Current'
C
      INDGR=53
      NLINE=1
      N(1)=ISTEP
      N(2)=ISTEP
      IOPT(1)=2
      IOPT(2)=2
C
      IF(IFLAG2 .NE. 1)THEN
        X(ISTEP)=SNGL(R*RO)
      DO 20 J=1,9
        Y(1,J,ISTEP)=SNGL(F(J))
        Y(2,J,ISTEP)=SNGL(DF(J))
        IF(J.EQ.1)THEN
        Y(2,1,ISTEP)=SNGL(XNUE(5))
        ENDIF
        IF(J.EQ.3)THEN
        Y(2,3,ISTEP)=SNGL(XNUE(1)+XNUE(2)+XNUE(3)+XNUE(4)+XNUE(5)
     $  +XNUE(6))
        Y(1,3,ISTEP)=SNGL(F(3)*POTO)
        ENDIF
        IF(J.EQ.5)THEN
        Y(1,5,ISTEP)=SNGL(F(5)*TEO)
        ENDIF
        IF(J.EQ.7)THEN
        Y(1,7,ISTEP)=SNGL(F(7)*EO)
        ENDIF
        IF(J.EQ.9)THEN
        Y(1,9,ISTEP)=SNGL(ABS(VE-VIC)/VE)
        ENDIF
```

```
        IF(J.EQ.2)THEN
        Y(2,2,ISTEP)=SNGL(XNUE(6))
        ENDIF
20    CONTINUE
C
C
      YSTORE(1,ISTEP)=SNGL(EVB)
      YSTORE(2,ISTEP)=SNGL(COLL)
      YSTORE(3,ISTEP)=SNGL(VE)
      YSTORE(4,ISTEP)=SNGL(VIC)
      YSTORE(5,ISTEP)=SNGL(CURE)
      YSTORE(6,ISTEP)=SNGL(CURIC)
C
      GO TO 100
C
      ELSE
C
        X(ISTEP)=SNGL(R*RO)
      DO 24 J=1,9
        Y(1,J,ISTEP)=SNGL(F(J))
        Y(2,J,ISTEP)=SNGL(DF(J))
        IF(J.EQ.1)THEN
        Y(2,1,ISTEP)=SNGL(XNUE(5))
        ENDIF
        IF(J.EQ.3)THEN
        Y(2,3,ISTEP)=SNGL(XNUE(1)+XNUE(2)+XNUE(3)+XNUE(4)+XNUE(5)
     $  +XNUE(6))
        Y(1,3,ISTEP)=SNGL(F(3)*POTO)
        ENDIF
        IF(J.EQ.5)THEN
        Y(1,5,ISTEP)=SNGL(F(5)*TEO)
        ENDIF
```

```
        IF(J.EQ.7)THEN
        Y(1,7,ISTEP)=SNGL(F(7)*EO)
        ENDIF
        IF(J.EQ.9)THEN
        Y(1,9,ISTEP)=SNGL(ABS(VE-VIC)/VE)
        ENDIF
        IF(J.EQ.2)THEN
        Y(2,2,ISTEP)=SNGL(XNUE(6))
        ENDIF
24    CONTINUE
C
C
      YSTORE(1,ISTEP)=SNGL(EVB)
      YSTORE(2,ISTEP)=SNGL(COLL)
      YSTORE(3,ISTEP)=SNGL(VE)
      YSTORE(4,ISTEP)=SNGL(VIC)
      YSTORE(5,ISTEP)=SNGL(CURE)
      YSTORE(6,ISTEP)=SNGL(CURIC)
C
      DO 12 I=1,ISTEP
        J=I+ISTEP
        Y(1,8,I)=YSTORE(1,I)
        Y(1,8,J)=YSTORE(2,I)
        Y(2,8,I)=YSTORE(3,I)
        Y(2,8,J)=YSTORE(4,I)
        Y(2,9,I)=YSTORE(5,I)
        Y(2,9,J)=YSTORE(6,I)
        X(J)=X(I)
12    CONTINUE
C
C
C***********************************************************************
```

```
C       THE FOLLOWING BLOCK CALCULATES THE ELECTRIC FIELD DERIVATIVE
C       BASED ON A TWO POINT, CENTRAL DIFFERENCE SCHEME. THIS
C       DERIVATIVE IS THEN USED TO EVALUATE THE QUOTIENT
C       (DENIC+DENIO-DENE)/DENE FOR PURPOSES OF CHECKING CONSISTENCY
C       OF ELECTRIC FIELD AND QUASINEUTRAL ASSUMPTION.
C
C***********************************************************************
C
C        DO 29 K=1,ISTEP
C        IF((K.GE.2).AND.(K.LE.(ISTEP-1)))THEN
C         DEDR(K)=(Y(1,7,K+1)-Y(1,7,K-1))/
C      $ (2.0*(X(K)-X(K-1)))*SNGL(DEDRO)/Y(1,6,K)
C         Y(1,9,K)=DEDR(K)
C        ELSE
C         DEDR(K)=0.0
C         Y(1,9,K)=DEDR(K)
C        ENDIF
C29      CONTINUE
C        Y(1,9,1)=Y(1,9,2)
C        Y(1,9,ISTEP)=Y(1,9,ISTEP-1)
C        Y(1,8,1)=Y(1,8,2)
C
26      NLINE=1
        WRITE(6,27)
27      FORMAT(' INPUT NUMBER FOR DESIRED PLOT')
        WRITE(6,61)
61      FORMAT(' 1  CONTACTOR NEUTRAL DENSITY')
        WRITE(6,62)
62      FORMAT(' 2  CONTACTOR ION DENSITY')
        WRITE(6,63)
63      FORMAT(' 3  POTENTIAL')
        WRITE(6,64)
```

```
64    FORMAT(' 4  HEAT FLUX')
      WRITE(6,65)
65    FORMAT(' 5  ELECTRON TEMPERATURE')
      WRITE(6,66)
66    FORMAT(' 6  ELECTRON DENSITY')
      WRITE(6,67)
67    FORMAT(' 7  ELECTRIC FIELD')
      WRITE(6,68)
68    FORMAT(' 8  EVB & COLL RATIO')
      WRITE(6,69)
69    FORMAT(' 9  RATIO OF DRIFT TO ELECTRON VELOCITIES')
      WRITE(6,71)
71    FORMAT(' 11 ION ACOUSTIC COLLISION RATE')
      WRITE(6,72)
72    FORMAT(' 12 BUNEMANN COLLISION RATE')
      WRITE(6,73)
73    FORMAT(' 13 TEMP CRITERIA FOR ION ACOUSTIC TURBULENCE')
      WRITE(6,74)
74    FORMAT(' 14 GRADIENT OF HEAT FLUX')
      WRITE(6,75)
75    FORMAT(' 15 GRADIENT OF ELECTRON TEMPERATURE')
      WRITE(6,76)
76    FORMAT(' 16 GRADIENT OF ELECTRON DENSITY')
      WRITE(6,77)
77    FORMAT(' 17 GRADIENT OF ELECTRIC FIELD')
      WRITE(6,78)
78    FORMAT(' 18 ELECTRON & ION DRIFT VELOCITY')
      WRITE(6,79)
79    FORMAT(' 19 ELECTRON & ION CURRENT')
      WRITE(6,70)
70    FORMAT(' 0  TO QUIT')
      READ(6,*) PCOM
```

```
C
      IF(PCOM.EQ.0)IFLAG3=1
      IF(IFLAG3.EQ.1)GO TO 100
C
      IF(PCOM.GT.10)THEN
      I=PCOM-10
      J=2
      ELSE
      I=PCOM
      J=1
      ENDIF
C
C
      DO 25 K=1,ISTEP
      YPL(K)=Y(J,I,K)
      IF((J.EQ.1).AND.(I.EQ.8)) YPL(K+ISTEP)=Y(1,8,K+ISTEP)
      IF((J.EQ.2).AND.(I.EQ.8)) YPL(K+ISTEP)=Y(2,8,K+ISTEP)
      IF((J.EQ.2).AND.(I.EQ.9)) YPL(K+ISTEP)=Y(2,9,K+ISTEP)
      IF((I.EQ.8).OR.((J.EQ.2).AND.(I.EQ.9))) NLINE=2
25    CONTINUE
      TITLE=TIT(I,J)
      PLOTITL=PLT(I,J)
      CALL GR_INIT(5,6,TITLE)
      CALL GR_LINE(IOPT,NLINE,PLOTITL,INDGR,X,YPL,N)
C
      GO TO 26
C
      ENDIF
C
100   CONTINUE
C
C
```

```
      RETURN
      END
C
```

A.3 Calculation of Potential and Density Gradients: GRAD

The subroutine GRAD evaluated all particle density gradients as well as the potential. In addition it calculated the ionization and recombination rates.

```
      SUBROUTINE GRAD(NEQ,R,F,DF)
      IMPLICIT REAL*8(A-H,O-Z)
      REAL*8 MP,MIC,ME,KAPPA,LAMBDAC,LAMBDAO,MASSIC,MIO,MASSIO,
     $       JIC,JIO,JE
      DIMENSION F(9),DF(9),XNUE(6)
      DATA PERMIT,B,EC,ME,MP/8.8542E-12,0.45E-4,1.6022E-19,
     $     9.1095E-31,1.67265E-27/
      COMMON/PARAM/CS,RO,DENICO,POTO,QDOTO,EO,TEO,SO,
     $ EISTAR,EESTAR,PSTAR,TESTAR,XNUE,EVB,CURICO,COLL,
     $ TIC,TIO,EIONC,EIONO,MIC,MIO,ZC,ZO,SIGENC,SIGENO,MASSIC,MASSIO,
     $ VE,VIC,VICO,POTO,DENIAMB,PI,KAPPA,CURT,CURE,CURIC,CURRAN,DEDRO,
     $ DENNC,DENIC,POT,QDOT,TE,DENE,E,DENIO,DENNO,BETA
C
      COMMON/GRAD/IONREC,JIC,JE,JIO,VEO,TEAMB
      COMMON/FLAG/ISTEP,IQUAS,IDIREC,ITURB
C
C
C*************************************************************************
C     IONIZATION AND RECOMBINATION RATES FOR AMBIENT AND CONTACTOR IONS
```

```
C
C*************************************************************************
C
      ERATC=EIONC/(TE*TEO)
      SIGVIC=(1.0E-5/DSQRT(ERATC)*EXP(-1.0*ERATC)/EIONC/DSQRT(EIONC)
     $       /(6.0+1.0/ERATC))*1.0E-6
      SIGVRC=(5.2E-14*DSQRT(ERATC)*(0.43+0.5*DLOG(ERATC)+0.469/ERATC
     $       **(1.0/3.0)))*1.0E-6
      IF(IONREC.EQ.1)THEN
       SIONC=DENNC*DENE*SIGVIC*DENICO**2
       SRECC=DENIC*DENE*SIGVRC*DENICO**2
      ELSE
       SRECC=0.0
       SIONC=0.0
      ENDIF
      S=(SIONC-SRECC)/SO
C
      VIC=DSQRT(VICO**2-2.0*PSTAR/EISTAR*(POT-POTO))
      CALL NUE(CCLASS,CEFF)
      VTHIC=9.79E+3/DSQRT(MASSIC)*DSQRT(TIC*TEO)/CS
      VTHIO=9.79E+3/DSQRT(MASSIO)*DSQRT(TIO*TEO)/CS
      KAPPA=3.2*DENE*TE*(TESTAR*DENICO/(ME*(CCLASS+CEFF)))
      XNU1=(XNUE(1)+XNUE(2)+XNUE(3)+XNUE(4)+XNUE(1)*VIC/VE)+CEFF
C
      IF(IQUAS.EQ.0)THEN
C
C
C     GRADIENT OF CONTACTOR NEUTRALS
C
      DF(1)=-2.0*DENNC/R
C
C     GRADIENT OF CONTACTOR IONS
```

```
C
      DF(2)=-(E*DENIC/VIC**2*(EC*EO*RO/EISTAR)+2*DENIC/R)
C
C     GRADIENT OF POTENTIAL
C
      DF(3)=-E*(EO*RO/POTO)
C
C     GRADIENT OF HEAT FLUX
C
C
      DF(4)=0.0
C
C     GRADIENT OF ELECTRON TEMPERATURE
C
       DF(5)=0.0
C
C     GRADIENT OF ELECTRON DENSITY
C
C
      DF(6)=E*DENE/VE**2*(EC*EO*RO/EESTAR)-2*DENE/R
C
C     GRADIENT OF RADIAL ELECTRIC FIELD
C
C
      DF(7)=(EC*RO*DENIAMB/(PERMIT*EO))*(DENIC+DENIO-DENE)-2.0*E/R
C
C
C     GRADIENT OF AMBIENT ION DENSITY
C
      IF(DABS(POT/TIO).LE. 50)THEN
       DF(8)=-(EO*RO/TEAMB)*EXP(-(POT*PSTAR)/(TIO*TESTAR))*E/TIO
      ELSE
```

```
      DF(8)=0.0
      ENDIF
C
C     GRADIENT OF AMBIENT NEUTRALS
C
        DF(9)=0.0
C
      ELSE
C
C
C*************************************************************************
C     FOLLLOWING EQUATIONS ARE FOR CALCULATION BASED ON
C     QUASINEUTRALITY IMPOSED EVERYWHERE.
C
C*************************************************************************
C
C     GRADIENT OF CONTACTOR NEUTRALS
C
      DF(1)=-S/VTHIC-2.0*DENNC/R
C
C     GRADIENT OF HEAT FLUX
C
      Q1=CURE*E/(4.0*PI*R**2)*(EO*CURICO/(QDOTO*RO))
      Q2=-3.0*DENE*(CCLASS+CEFF)*(TE-TIC)*(ME/MIC*TESTAR*RO*
     $    DENICO/QDOTO)
      Q3=-EIONC*SIONC*EC*RO/QDOTO
      Q4=-2.0*QDOT/R
C
      DF(4)=Q1+Q2+Q3+Q4
C
C
C     GRADIENT OF ELECTRON TEMPERATURE
```

```
C
      IF(TE.GT.1.0)THEN
       DF(5)=-QDOT*(QDOTO*RO/(KAPPA*EC*TEO))
      ELSE
       DF(5)=0.0
      ENDIF
C
C     GRADIENT OF CONTACTOR IONS
C
       BO=1.0/(VIC**2)*(DENIC/DENE)*(EESTAR/EISTAR)
       B1=S/VIC
       B2=-2.0*DENIC/R
       B3=BO*VE*S
       B4=BO*TESTAR*DENE/EESTAR*DF(5)
       B5=-BO*DENE*VE*RO/CS*XNU1
       B6=1.0-BO*(TE*(TESTAR/EESTAR)-(VE**2))
C
       DF(2)=(B1+B2+B3+B4+B5)/B6
C
C
C     GRADIENT OF POTENTIAL
C
       C1=DF(2)*(TE*(TESTAR/EESTAR)-(VE**2))*EESTAR/(PSTAR*DENE)
       C2=VE*S*EESTAR/(DENE*PSTAR)
       C3=DF(5)*(TESTAR/PSTAR)
       C4=-VE*(RO/CS)*(EESTAR/PSTAR)*XNU1
C
       DF(3)=C1+C2+C3+C4
C
C
C
C     GRADIENT OF ELECTRON DENSITY
```

```
C
      DF(6)=DF(2)
C
C     GRADIENT OF RADIAL ELECTRIC FIELD
C
      DF(7)=(DENIC+DENIO-DENE)*(EC*DENICO*RO/(PERMIT*EO))-2.0*E/R
C
C     GRADIENT OF AMBIENT ION DENSITY
C
        DF(8)=0.0
C
C     GRADIENT OF AMBIENT NEUTRALS
C
        DF(9)=0.0
C
      ENDIF
C
      RETURN
      END
C
C
```

A.4 Calculation of Collision Frequencies: NUE

The subroutine NUE calculated the collision frequencies as well as the collisionality parameter.

```
      SUBROUTINE NUE(CCLASS,CEFF)
      IMPLICIT REAL*8(A-H,O-Z)
      REAL*8 MP,MIC,ME,KAPPA,LAMBDAC,LAMBDAO,MASSIC,MIO,MASSIO
```

```
      DIMENSION XNUE(6)
      DATA PERMIT,B,EC,ME,MP/8.8542E-12,0.45E-4,1.6022E-19,
     $     9.1095E-31,1.67265E-27/
      COMMON/PARAM/CS,RO,DENICO,POTO,QDOTO,EO,TEO,SO,
     $ EISTAR,EESTAR,PSTAR,TESTAR,XNUE,EVB,CURICO,COLL,
     $ TIC,TIO,EIONC,EIONO,MIC,MIO,ZC,ZO,SIGENC,SIGENO,MASSIC,MASSIO,
     $ VE,VIC,VICO,POTO,DENIAMB,PI,KAPPA,CURT,CURE,CURIC,CURRAN,DEDRO,
     $ DENNC,DENIC,POT,QDOT,TE,DENE,E,DENIO,DENNO,BETA
      COMMON/FLAG/ISTEP,IQUAS,IDIREC,ITURB
C
C
      XNUE(5)=0.0
      XNUE(6)=0.0
C
      TRATC=TE/TIC
      VD=(VIC*DENIC/DENE+VE)
      VTHE=4.19E+5*DSQRT(TE*TEO)
      VCRIT=1.0/DSQRT(2.DO)*(1.0+DSQRT(TRATC*MIC/ME)
     $      *TRATC*EXP(-0.5*(3.0+TRATC)))
      OMEGA=5.64E+4*DSQRT(DENE*DENICO*1.E-6)
      LAMBDAC=23-DLOG(DSQRT(DENE*DENICO*1.E-6)*ZC*TE*TEO**(-1.5))
      LAMBDAO=23-DLOG(DSQRT(DENE*DENICO*1.E-6)*ZO*TE*TEO**(-1.5))
C
      XNUE(1)=3.9E-6*TE*TEO**(-1.5)*(DENIC*DENICO*1.E-6)*ZC**2.0*LAMBDAC
      XNUE(2)=3.9E-6*TE*TEO**(-1.5)*(DENIO*DENICO*1.E-6)*ZO**2.0*LAMBDAO
C
      XNUE(3)=DENNC*DENICO*SIGENC*VTHE
      XNUE(4)=DENNO*DENICO*SIGENO*VTHE
C
      CCLASS=XNUE(1)+XNUE(2)+XNUE(3)+XNUE(4)
C
      IF(ITURB.EQ.1)THEN
```

```
C
      IF(VD .GT. VCRIT) XNUE(5)=0.01*TRATC*VE*CS/VTHE*OMEGA
      EDRI=ME/EC*(CCLASS+XNUE(5))*VTHE/EO
      IF(E .GT. EDRI) XNUE(6)=0.53*(ME/MIC)**0.61*OMEGA
C
      ENDIF
C
      CEFF=XNUE(5)+XNUE(6)
C
      IF(BETA .GE. 1.0)THEN
        COLL=100.0
        ELSE
        BMOD=DSQRT(1-BETA)*B
        COLL=1.0/(2.8025E+10*BMOD/(CCLASS+CEFF))
      ENDIF
C
      RETURN
      END
C
C
```

A.5 Jacobian: JAC

One input of the LSODE ODE solver is the Jacobian of the system of equations being solved. The following subroutine was a dummy routine since the Jacobian was calculated within the LSODE routine itself. A user supplied Jacobian is an option with this package however.

```
      SUBROUTINE JAC
C
```

```
C*************************************************************************
C     THE JACOBIAN FOR THIS SYSTEM IS CURRENTLY CALCULATED
C     WITHIN THE LSODE ROUTINE
C
C*************************************************************************
      RETURN
      END
```

A.6 Data Input

Below is a listing of the input data file for the contactor program. The meaning of the various variables is defined in the main program ITETHER. The values shown below correspond to the default case.

```
$INPUTDAT
 CURICO=1.0
 CUREO=0.0
 POTO=0.0
 EO=0.0
 TEO=0.5
 DENEO=0.0
 QDOTO=0.0
 VICOO=0.0
 RO=0.1
 RFIN=10.0
 TEAMB=0.1  DENIAMB=2.0E+12
 MASSIO=16.0 EIONO=13.62 TIOO=0.1 SIGENO=2.5E-20 FRACIO=2.0E-4 ZO=1.0
```

```
MASSIC=40.0 EIONC=15.76 TICO=0.1 SIGENC=8.0E-20 FRACIC=1.0E-1 ZC=1.0
STEPFAC=0.025
IPLOT=1 STPSTOP=9000
IQUAS=1 IDIREC=0 INTER=1
MACHION=1.0
DENFAC=1.0
ITURB=1
HIFAC=10.0
IONREC=1
ISTOP=1
$
```

Bibliography

[1] S. I. Braginski. Transport processes in a plasma. In *Rev. of Plasma Phys.*, Consultants Bureau, 1965.

[2] M. Dobrowolny and L. Iess. Model of the interaction of a hollow cathode with the ionosphere. 1987. in *Second International Conference on Tethers in Space.* American Institute of Aeronautics and Astronautics, 1988.

[3] G. Vannaroni et. al. Experimental characterization of hollow cathode plasma sources at Frascati. 1987. in *Space Tethers for Science in the Space Station Era.* Italian Society of Physics, v14.

[4] D. E. Hastings. Theory of plasma contactors used in the ionosphere. *J. Spacecraft and Rockets*, 24:250–256, 1987.

[5] D. E. Hastings and J. Blandino. Bounds on current collection by plasma clouds from the ionoshphere. 1988. accepted for publication by *J. Geophys. Res.* on 12/1/88.

[6] D. E. Hastings and N. A. Gatsonis. Physics of plasma contactor clouds used for electron collection in space. *Acta Astronautica*, 17:827–836, 1988.

[7] O. Ishihara, A. Hirose, and A. B. Langdon. Nonlinear evolution of the Buneman instability. *Phys. of Fluids*, 24:452–464, 1981.

[8] I. Katz and A. Davis. On the need for space tests of plasma contactors as plasma collectors. in *Second International Conference on Tethers in Space.* American Institute of Aeronautics and Astronautics, 1988.

[9] I. Katz and D. Parks. Theory of plasma contactors for electrodynamic tethered satellite systems. *J. Spacecraft and Rockets*, 24:245–249, 1987.

[10] M. Martinez-Sanchez and D. E. Hastings. A systems study of a 100 kW tether. *J. of Astronautical Sciences*, 35:75–96, 1987.

[11] R. W. P. McWhirter. Spectral intensities. In R. H. Huddleston and S.L. Leonard, editors, *Plasma Diagnostic Techniques*, Academic Press, New York, 1965.

[12] K. Papadopoulos. A review of anomalous resistivity for the ionosphere. *Rev. of Geophys. and Space Phys.*, 15:113–127, 1977.

[13] D. Parks and I. Katz. Theory of plasma contactors for electrodynamic tethered satellite systems. *J. Spacecraft and Rockets*, 24:245–249, 1987.

[14] M. J. Seaton. Radiative recombination of hydrogen ions. *Monthly Notices of the Royal Astronomical Society*, 119:81, 1959.

[15] J. P. Lebreton et al. Laboratory model of a tethered satellite: current collection upon and sheath formation around a charged body in a drifting magnetoplasma. *Adv. Space Res.*, 8:213–220, 1988.

[16] R. Wei and P. Wilbur. Space-charge limited current flow in a spherical double sheath. *J. Applied Phys.*, 60:2280–2284, 1986.

[17] J. Williams P. Wilbur and J. Monheiser. *Experimental Validation of a Phenomenological Model of the Plasma Contacting Process.* Technical Report NASA CR-182148, NASA Lewis Research Center, 1988. Space Plasma Contactor Research Annual Report APPENDIX A.

[18] J. Williams and P. Wilbur. *An Experimental Investigation of the Plasma Contacting Process.* Technical Report NASA CR-182148, NASA Lewis Re-

search Center, 1988. Space Plasma Contactor Research Annual Report

APPENDIX B.